Galaxy Publication

A Validated Whole-Body PBPK Model of Dextromethorphan and Its Metabolites for Genotype-Based Prediction of CYP2D6 Phenotype and Urinary Metabolic Ratio

Khaled Musa[1], Othman Noor[1]*, Mustafa Ibrahim[1], Anwar Saleh[1]

[1]Department of Natural Products Research, Faculty of Pharmacy, International Islamic University Malaysia, Kuantan, Malaysia.

*E-mail ✉ othman.noor.np@gmail.com

ABSTRACT

Cytochrome P450 2D6 (CYP2D6) is a major enzyme responsible for processing xenobiotics and contributes to the elimination of numerous therapeutic agents. Variation in the CYP2D6 gene produces substantial person-to-person differences in metabolic capacity and can influence how CYP2D6 probe compounds, such as dextromethorphan (DXM), are phenotyped. To explore these effects, we (i) assembled a large DXM pharmacokinetic dataset and (ii) created and verified a physiologically based pharmacokinetic (PBPK) model describing DXM and its metabolites—dextrorphan (DXO) and dextrorphan O-glucuronide (DXO-Glu). Drug–gene interactions (DGI) were incorporated by adjusting CYP2D6 kinetic parameters according to the activity score (AS), enabling simulation of individual genotypes through AS combinations. Variation in CYP3A4 and CYP2D6 activities was characterized using human liver microsome data. The resulting simulations closely replicate observed pharmacokinetics for CYP2D6 genotypes, AS-defined activity levels, and metabolic phenotypes (UM, EM, IM, PM). Using this framework, we examined genotype–phenotype relationships and assessed how CYP2D6 variants affect phenotyping, quantified by the urinary cumulative metabolic ratio (UCMR), defined as DXM/(DXO + DXO-Glu). Sensitivity analyses were used to determine which factors most strongly influence UCMR. Model outputs show high resilience to different dosing procedures (formulation, dose, dissolution, sampling schedule) and to physiological variability. The approach can estimate UCMR distributions in and across populations as a function of AS, and can also predict the likelihood of genotype–phenotype misclassification when allele frequencies are known. It supports individualized prediction of both UCMR and metabolic phenotype from CYP2D6 genotype. All datasets and model files are publicly accessible.

Keywords: Dextromethorphan (DXM), CYP2D6, PBPK modeling, Pharmacokinetics, Pharmacogenomics (PGx), Metabolic phenotype

Introduction

The cytochrome P450 (CYP) family is vital for processing a wide range of chemicals and pharmaceuticals. Among its members, CYP2D6 plays a prominent role, participating in the metabolism of roughly 20% of frequently prescribed medications [1]. This includes antiarrhythmic drugs with narrow safety ranges (flecainide, procainamide, mexiletine), anticancer agents (tamoxifen), antidepressants (citalopram, fluoxetine, duloxetine, venlafaxine), antipsychotics (aripiprazole, haloperidol, thioridazine), β-blockers (metoprolol), opioid and non-opioid analgesics (tramadol, oxycodone, codeine), and antitussives (dextromethorphan) [2, 3]. Drug responses driven by CYP2D6 show striking variability, complicating dose selection and raising risks of therapeutic failure or toxicity. This variation is strongly influenced by genetic differences [4–6], with certain alleles linked to adverse reactions, lack of efficacy, and even fatal intoxication [7–10].

**In the late 1970s, unusual patterns in debrisoquine hydroxylation [11] and sparteine oxidation [12] led to the recognition of CYP2D6 polymorphism. Since then, CYP2D6 has become one of the most analyzed drug-

metabolizing enzymes. Early classifications grouped individuals with particular genotypes into poor (gPM), intermediate (gIM), extensive (gEM), or ultrarapid metabolizers (gUM) [13, 14]. We use the prefix 'g' to distinguish these genetically predicted categories from phenotypes determined experimentally via probe-drug pharmacokinetics. The more detailed activity score (AS) framework, which assigns each allele a value from 0 to 1, is now commonly used to link genotype with metabolic function [15]. The total AS equals the sum of the scores of both alleles—for example, an individual with 1/3 (AS of 1 and 0) receives an AS of 1. Copy-number variation, hybrid genes, and CYP2D7-related rearrangements can complicate diplotype interpretation [16–18]. AS recommendations are periodically revised [19]. Numerous population studies have identified how alleles are distributed and how they influence metabolic traits [14]. More than 130 CYP2D6 star-allele haplotypes have been documented by the PharmVar Consortium and incorporated into PharmGKB with their AS contributions [20, 21]. A variety of approaches are used for metabolic phenotyping with probe drugs. The classical strategy involves collecting plasma concentrations of a probe compound and its metabolites at several intervals after dosing. From these concentration-time curves, one can derive (partial) clearance values and estimate relative enzyme activities. For many probes, simplified procedures have been introduced that avoid repeated blood draws; instead, single-sample metabolic ratios—comparing the parent drug with one or more metabolites in plasma, blood, or urine—serve as surrogate indicators. Large cohort studies commonly rely on urinary metabolite ratios. Other biological matrices, such as saliva or exhaled breath, may also be suitable [22]. Substances used to phenotype CYP2D6 include debrisoquine, dextromethorphan, metoprolol, and sparteine [23, 24]. Bufuralol, although less frequently applied clinically, is useful in vitro because of its fluorescence [13]. Debrisoquine and sparteine perform well as CYP2D6 probes, yet their withdrawal from routine clinical use in many countries limits access to them. Metoprolol and dextromethorphan are therefore the most commonly applied alternatives for CYP2D6 activity assessment.

Dextromethorphan (DXM) is an over-the-counter antitussive, structurally related to codeine, that modulates several neural receptors and ion channels involved in suppressing cough [25]. It is widely available, viewed as safe at therapeutic doses, and generally well tolerated [24]. Beyond clinical use, DXM is widely adopted as a CYP2D6 probe, either alone or within multi-probe cocktails. DXM can be given orally or intravenously, exhibits low oral bioavailability (≈50%), and undergoes extensive first-pass metabolism in the gut and liver. Typically, only around half the administered dose appears in urine within at least 12 h, largely as glucuronide products [26–29]. In circulation, roughly 55–65% of DXM is non-specifically associated with plasma proteins [30, 31].

DXM metabolism occurs predominantly in the liver, where CYP2D6 converts it via O-demethylation to dextrorphan (DXO). Most DXO is then rapidly glucuronidated by UGT enzymes to form dextrorphan O-glucuronide (DXO-Glu), which is excreted in urine. In individuals lacking functional CYP2D6 alleles, the formation of DXO is extremely slow but not completely absent. O-demethylation is therefore not strictly CYP2D6-dependent; in vitro evidence shows that CYP3A4, CYP3A5, and CYP2C9 can perform this reaction to a limited extent [32–35]. Consistent with this, blocking CYP2D6 has minimal impact in poor metabolizers [36]. A second metabolic route involves N-demethylation to 3-methoxymorphinan, mainly via CYP3A4. Both 3-methoxymorphinan and DXO are further converted to 3-hydroxymorphinan, which is then glucuronidated to hydroxymorphinan O-glucuronide and eliminated in urine. The urinary cumulative metabolic ratio (UCMR), defined as DXM/(DXO + DXO-Glu), is widely used for in vivo CYP2D6 phenotyping.

A key issue in phenotyping and liver function analysis is understanding how CYP2D6 genetic variation influences DXM pharmacokinetics and DXM-based phenotyping metrics such as the UCMR. The aim of this study was to address this using physiologically based pharmacokinetic (PBPK) modeling of DXM.

Materials and Methods

Pharmacokinetics database of DXM
We compiled pharmacokinetic data on DXM from published studies to support model development, refinement, and evaluation. The curation primarily targeted concentration-time curves for DXM, DXO, and DXO-Glu in plasma or serum, as well as urinary amounts and metabolic ratios. Metadata describing study participants (e.g., CYP2D6 genotype or activity score) and study design (e.g., DXM dose and formulation) were recorded. All information was collected using an established curation workflow [37] and is publicly available in the PK-DB pharmacokinetics repository (https://pk-db.com) [38]. Initially, a PubMed search was conducted using the query:

https://pubmed.ncbi.nlm.nih.gov/?term=dextromethorphan+AND+%28phenotype+OR+phenotyping%29+AND +genotype. The dataset was expanded with cocktail-study records from PK-DB [37], additional references, and data identified through PKPDAI using the search string: https://app.pkpdai.com/?term=dextromethorphan [38]. Publications were screened and curated based on predefined eligibility rules. Throughout curation, new relevant papers were incorporated from citation networks. Some studies reported only summary pharmacokinetic parameters without full time profiles; these were curated but excluded from subsequent modeling analyses.

To qualify for inclusion, reports needed to present in vivo pharmacokinetic observations in adult participants (≥18 years) who had received dextromethorphan (DXM) or DXM hydrobromide. Only oral (PO) and intravenous (IV) dosing routes were considered, but any formulation type (e.g., capsules, tablets, liquids) was acceptable. No limits were introduced regarding dose size or any coadministered agents. During model assembly, studies involving substances that altered DXM disposition through metabolic inhibition or induction were identified and removed. Required data types included time-course concentration measurements in plasma or serum, urinary recovery of DXM and metabolites, and metabolite-to-metabolite ratios such as UCMR. Publications reporting pharmacokinetic parameters (AUC, half-life, clearance) or cumulative urinary ratios for DXM and its metabolites were also considered. Datasets providing full temporal profiles together with CYP2D6 genotype information were especially valued. Studies involving subjects with medical conditions known to influence the handling of DXM or its metabolites were excluded. Study B from Frank's 2009 dissertation diverged markedly from all other datasets and was removed. Additionally, Wyen *et al.* (2008) were determined to replicate Study E from Frank (2009) and were excluded [39, 40]. The finalized list of studies used in the evaluation appears in **Table 1**.

Table 1. Human studies are used for pharmacokinetic model assessment.

Reference	PK-DB	PMID	DXM Application	Dosing Protocol	Description
Abdelrahman *et al.* (1999) [41]	PKDB00573	10340911	DXM	Oral syrup: 0.3 mg/kg	Study examining how terbinafine acts as an in vivo CYP2D6 blocker
Abduljalil *et al.* (2010) [42]	PKDB00574	20881950	DXM hydrobromide	Oral capsule: 30 mg	Population PK analysis used to quantify activity levels of CYP2D6*1, *2, and *41 variants via dextromethorphan
Armani *et al.* (2017) [43]	PKDB00428	10340911	DXM (cocktail)	Oral (NR): 30 mg	Work evaluating antitussive outcomes of dextromethorphan relative to CYP2D6 activity
Barnhart (1980) [44]	PKDB00575	7423506	DXM hydrobromide	Oral capsule: 30 mg	Comparison of urinary excretion patterns for DXM and three metabolites in dogs and humans
Capon *et al.* (1996) [27]	PKDB00576	8841152	DXM hydrobromide	Oral (NR): 30 mg	Assessment of cough suppression effects of DXM in relation to CYP2D6 function
Chen *et al.* (2017) [45]	PKDB00577	28512430	DXM	Oral tablet: 15 mg + 300 ml water	Use of plasma, urine, and saliva metabolic ratios for CYP2D6 phenotyping and evaluation of CYP2D6*10 variability in a Chinese cohort
Chládek *et al.* (2000) [46]	PKDB00578	11214771	DXM hydrobromide	Oral syrup: 30 mg	Comparison of 4-hour urine and 3-hour plasma metabolic ratios as CYP2D6 indicators
Demirbas *et al.* (1998) [47]	PKDB00579	9840216	DXM hydrobromide	Oral sustained-release tablet: 60 mg	Bioavailability evaluation of DXM (as dextrorphan) from extended-release formulations co-administered with guaifenesin
Dorado *et al.* (2017) [48]	PKDB00580	28271978	DXM	Oral (NR): 15 mg	Cuban data highlighting that CYP2D6 genotype alone does not reliably predict ultrarapid metabolism
Doroshyenko *et al.* (2013) [49]	PKDB00138	23401474	DXM (cocktail)	Oral capsule: 30 mg	Investigation of drug biotransformation and disposition characteristics
Duedahl *et al.* (2005) [50]	PKDB00597	15661445	DXM	Intravenous: 0.5 mg/kg	IV DXM study linking PK behavior with its anti-hyperalgesic properties

|					
Dumond *et al.* (2010) [51]	PKDB0 0499	20147896	DXM (cocktail)	Oral solution: 30 mg	Genotype–phenotype approach for predicting drug interactions involving CYP450 and P-gp during tipranavir/ritonavir treatment
Edwards *et al.* (2017) [52]	PKDB0 0496	28808886	DXM (cocktail)	Oral capsule: 30 mg	PK interaction investigation involving obeticholic acid and multiple probe substrates including DXM
Eichhold *et al.* (1997) [53]	PKDB0 0596	–	DXM hydrobromide	Oral syrup: 30 mg	LC–MS/MS quantification of DXM and dextrorphan in plasma
Eichhold *et al.* (2007) [54]	PKDB0 0581	16930908	DXM hydrobromide	Oral solution: 20 mg	Simultaneous plasma determination of DXM, dextrorphan, and guaifenesin using semi-automated extraction and LC–MS/MS
Frank (2009) [40]	PKDB0 0582	–	DXM hydrobromide (cocktail)	Oral capsule: 30 mg	Evaluation of PK markers used for CYP2D6 phenotyping with DXM
Gaedigk (2013) [55]	PKDB0 0583	24151800	DXM	Oral syrup: 0.3 mg/kg	Discussion of analytical complexities in interpreting CYP2D6 genotypes
Hou *et al.* (1991) [56]	PKDB0 0584	2015730	DXM hydrobromide	Oral capsule: 50 mg	Saliva-based assessment of DXM metabolic phenotype
Hu *et al.* (2011) [57]	PKDB0 0585	21050887	DXM hydrobromide	Oral sustained-release tablet: 30 mg	Evaluation of a gas-forming floating matrix DXM system in vitro and in vivo
Jones *et al.* (1996) [58]	PKDB0 0586	8873685	DXM hydrobromide	Oral syrup: 30 mg	Measurement of CYP3A4/5 activity using DXM N-demethylation
Köhler *et al.* (1997) [59]	PKDB0 0587	9429230	DXM	Oral syrup: 20 mg	Genotype–phenotype comparison using serum DXM and metabolite levels in healthy controls and psychiatric patients
López *et al.* (2005) [60]	PKDB0 0588	16249913	DXM hydrobromide	Oral syrup: 30 mg	Determination of CYP2D6 genotype and phenotype in Mexican Mestizo subjects
Lenuzza *et al.* (2016) [61]	PKDB0 0598	25465228	DXM (cocktail)	Oral tablet: 18 mg	PK and safety evaluation of a combined drug/metabolite panel (CIME) after single dosing
Montané Jaime *et al.* (2013) [62]	PKDB0 0589	23394389	DXM hydrobromide	Oral (NR): 30 mg + water	Characterization of CYP2D6 gene structure and metabolic activity in Indo- and Afro-Trinidadian groups; discovery of novel alleles
Myrand *et al.* (2008) [63]	PKDB0 0497	18231117	DXM (cocktail)	Oral (NR): 30 mg	PK–genotype correlations for major CYP enzymes in Japanese, compared with Korean, Chinese, and Caucasian populations
Nagai *et al.* (1996) [64]	PKDB0 0590	8830977	DXM hydrobromide	Oral tablet: 30 mg	PK characteristics and polymorphic oxidation of DXM in Japanese individuals
Nakashima *et al.* (2007) [65]	PKDB0 0599	17652181	DXM hydrobromide	Oral tablet: 30 mg	Influence of cinacalcet hydrochloride on DXM PK in vitro and in clinical settings
Nyunt *et al.* (2008) [66]	PKDB0 0591	18362694	DXM	Oral tablet: 30 mg	Effect of the CXCR4 antagonist AMD070 on CYP3A4 and CYP2D6 probe drugs including DXM
Oh *et al.* (2012) [67]	PKDB0 0054	22483397	DXM (cocktail)	Oral (NR): 2 mg	Highly sensitive LC–MS/MS method for simultaneous detection of five P450 substrates and metabolites
Pope *et al.* (2004) [36]	PKDB0 0592	15342614	DXM	Oral capsule: 30 mg; 45 mg; 60 mg	Single- and multiple-dose PK evaluation of DXM with quinidine in extensive and poor metabolizers

Qiu *et al.* (2016) [68]	PKDB00600	27023460	DXM hydrobromide	Oral tablet: 15 mg	Assessment of "Zuojin Pill" effects on DXM PK in healthy Chinese carriers of CYP2D6*10
Schadel *et al.* (1995) [26]	PKDB00593	7593709	DXM	Oral capsule: 30 mg	PK behavior of DXM and metabolites in relation to CYP2D6 phenotype and quinidine inhibition
Schoedel *et al.* (2012) [69]	PKDB00594	22283559	DXM	Oral capsule: 30 mg twice daily for 8 days	Open-label DDI trial exploring DXM/quinidine interactions with paroxetine
Tamminga *et al.* (2001) [70]	PKDB00498	11829201	DXM hydrobromide	Oral tablet: 22 mg	Frequencies of CYP2D6 and CYP2C19 genotypes in Dutch volunteers
Yamazaki *et al.* (2017) [71]	PKDB00494	27273149	DXM (cocktail)	Oral (NR): 30 mg	PK influence of isavuconazole when co-administered with probe substrates such as DXM
Zawertailo *et al.* (2010) [72]	PKDB00595	20041473	DXM	Oral capsule: 3 mg/kg	Examining how metabolic inhibition alters the psychoactive responses to DXM

NR = not reported; DXM = dextromethorphan.

The approach for identifying and evaluating the literature adapted elements of the PRISMA-ScR framework [73]. The initial search returned 404 records. Following screening, application of the eligibility rules, and prioritization, 47 studies were curated, of which 36 contributed data used in this work **(Table 1)**.

PBPK model of DXM

A physiologically based pharmacokinetic representation of DXM, DXO, and DXO-Glu **(Figure 1)** was created using the Systems Biology Markup Language (SBML) [74, 75]. Construction and visualization relied on sbmlutils [76] and cy3sbml [77, 78]. The model consists of ordinary differential equations, solved computationally with sbmlsim [79], which employs libroadrunner as the underlying SBML solver [80, 81]. The SBML implementation (CC-BY 4.0) is publicly accessible, and the analyses herein relied on version 0.9.5 [82].
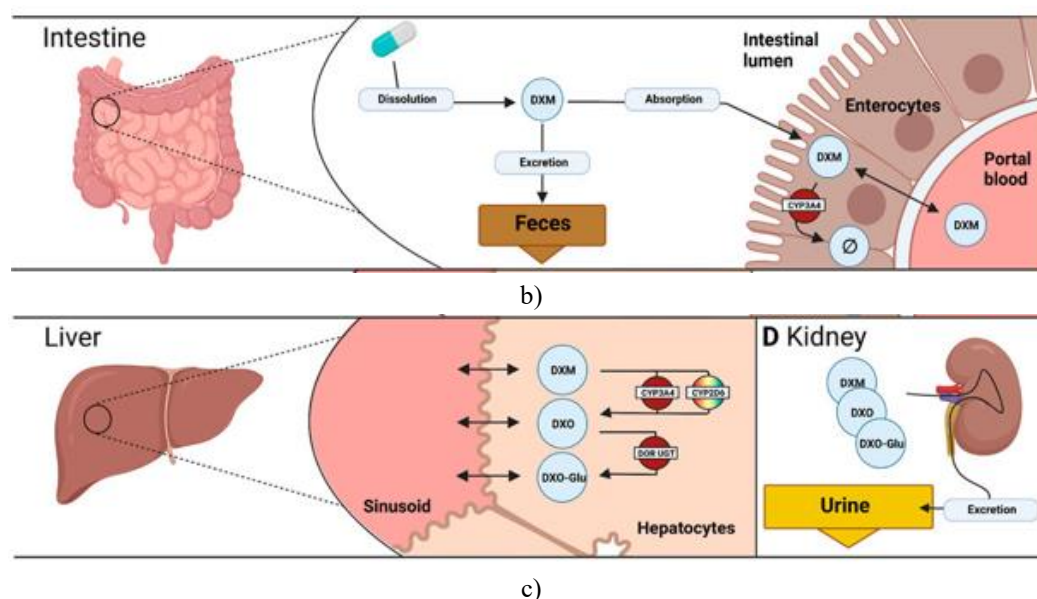

a)

b)

c)
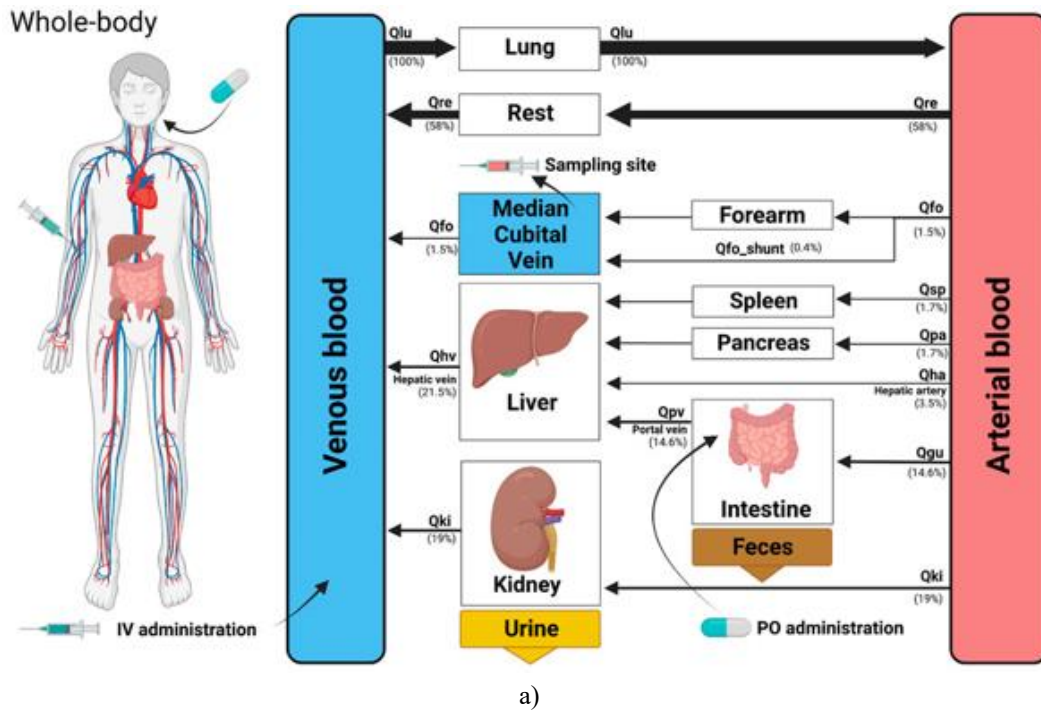
Figure 1. Model schematic for DXM.

(a) Whole-body arrangement including liver, kidney, intestine, forearm, lung, and a generalized rest compartment into which low-impact tissues are grouped. Compartments exchange through systemic blood flow, with flow magnitudes indicated by arrow thickness. DXM enters via IV infusion (venous compartment) or PO dosing (intestinal compartment). (b) Intestinal module representing dissolution, absorption, and fecal elimination. Only part of the oral dose becomes systemically available; the remainder is lost through feces. CYP3A4-mediated first-pass metabolism in the gut reduces the amount reaching circulation. (c) Hepatic processes involving conversion of DXM to DXO by CYP2D6 (primary) and CYP3A4 (secondary), followed by glucuronidation to DXO-Glu. (d) Renal handling describing urinary removal of DXM, DXO, and DXO-Glu.

The model uses a hierarchical organization [83], with the upper level detailing whole-body physiology and the lower level describing drug-specific processes. Tissues expected to exert minimal influence are merged into a rest compartment. IV doses enter the venous section, whereas oral doses appear in the gastrointestinal tract. Only a fraction of the ingested DXM passes into the blood; the unrecovered portion exits through fecal elimination. Plasma profiles correspond to concentrations sampled from the median cubital vein.
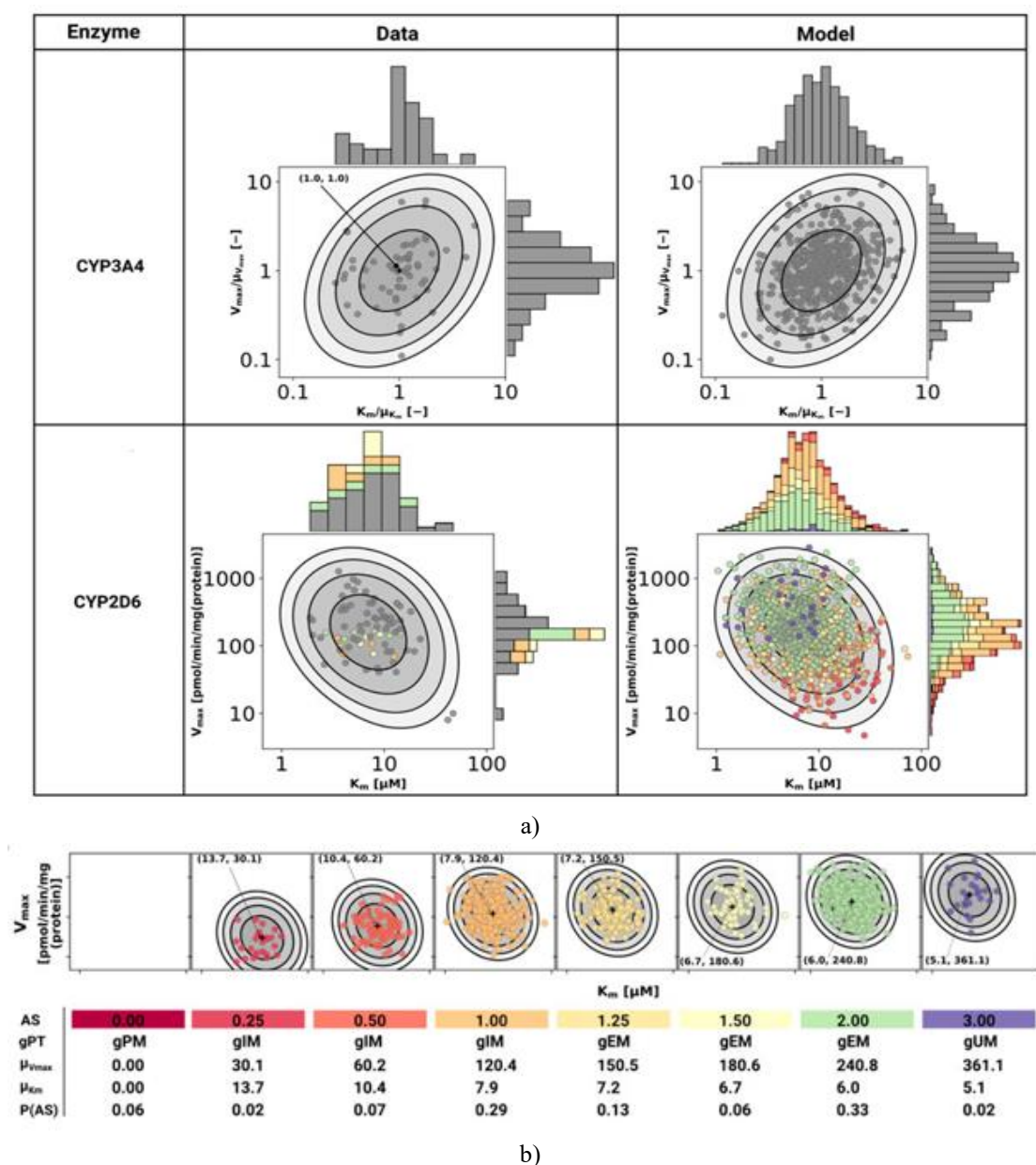
Distribution of DXM, DXO, and DXO-Glu among tissues and plasma is determined by tissue-to-plasma partition coefficients (Kp) together with distribution rate constants (f_tissue).

Only pathways essential for reproducing available pharmacokinetic results were retained **(Figures 1b and 1c)**. Minor processes—including hepatic N-demethylation—were not modeled. Intestinal and hepatic biotransformation steps follow irreversible Michaelis–Menten kinetics, $v = V_{max} \cdot S / (S + K_m)$, with V_{max} and K_m for CYP2D6 and CYP3A4 sampled from designated distributions. Formation of DXO in the liver may occur through either CYP2D6 or CYP3A4, though the former dominates. Any reaction producing compounds outside the DXM → DXO → DXO-Glu pathway was represented as an annihilation step, meaning such products were not tracked further. Renal excretion accounts for the elimination of DXM, DXO, and DXO-Glu.

A subset of model parameters was optimized by minimizing discrepancies between simulations and the experimental datasets shown in **Figures 4–9**.

CYP3A4 and CYP2D6

Inter-individual differences in CYP3A4 and CYP2D6 were represented using paired lognormal distributions, linked through correlation, and constructed from published in vitro measurements for CYP2D6 [83, 84] and CYP3A4 [84]. After applying a log10 conversion, a Gaussian model characterized by its mean (μ) and standard deviation was estimated via maximum likelihood. A Gaussian copula, parameterized with Kendall's tau obtained from the experimental datasets, was used to generate the joint distribution **(Figure 2)**.

a)

b)

Figure 2. Representation of CYP3A4 and CYP2D6.

(a) The distributions of both enzymes are shown. Biotransformation of DXM to DXO mediated by CYP3A4 and CYP2D6 was described with Michaelis–Menten equations. Inter-subject variation was incorporated as two-dimensional lognormal distributions for K_m and V_{max}. Parameter sets were obtained by fitting to human liver microsome measurements. CYP3A4 variability was derived from midazolam experiments [83], and CYP2D6 variability from DXM-based assays [84, 85]. To translate midazolam-derived CYP3A4 data to DXM, normalized values were applied. The CYP2D6 distribution was formulated as a mixture aligned with activity scores, as displayed in (b). Each sample corresponds to a $V_{max} - K_m$ pair, with CYP2D6 points colored according to activity score.

(b) CYP2D6 activity-score scheme. Activity categories were reproduced through a mixture model. Higher activity scores correspond to increased V_{max} for conversion of DXM → DXO and lower μ K_m, indicating enhanced catalytic capacity and substrate affinity. The provided table lists AS, genetic phenotype (gPT), average V_{max}, average K_m, and the AS prevalence from curated UCMR datasets (P(AS)). AS = 0.0 signifies an absence of measurable CYP2D6-mediated DXM → DXO metabolism.

To reflect activity score effects, V_{max} was scaled proportionally to AS ($V_{max} \propto$ AS), and K_m was adjusted along the first principal component derived from $\log10(K_m)$ and $\log10(V_{max})$ (principal component regression).

Genotype effects were incorporated by assigning AS values to CYP2D6 allelic variants and summing the contributions of both alleles. AS–allele mappings followed PharmGKB (https://www.pharmgkb.org/page/cyp2d6RefMaterials, accessed 2022-01-10) [21].

The population-level CYP2D6 kinetic model was constructed as a weighted mixture of AS-specific models:

$$P(V_{max}, K_m) = \sum_{AS} P(AS)P(V_{max}, K_m|AS) \tag{1}$$

Simulations for any AS used the corresponding $V_{max} - K_m$ pair **(Figure 2)**. Variability was produced by drawing V_{max} and K_m values from the independent CYP3A4 and CYP2D6 distributions. For population-dependent predictions, biogeographical AS frequencies from PharmGKB (accessed 2022-01-10) [21] were applied.

CYP2D6 metabolic phenotype
Phenotypic groups—ultrarapid (UM), extensive (EM), intermediate (IM), and poor metabolizers (PM)—were defined according to the urinary cumulative metabolic ratio UCMR = DXM / (DXO + DXO-Glu). Cutoff values used were: PM: UCMR ≥ 0.3; IM: 0.03 ≤ UCMR < 0.3; EM: 0.0003 ≤ UCMR < 0.03; UM: UCMR < 0.0003. Studies describing "normal metabolizers (NM)" with identical thresholds to EM were treated as EM.

Sensitivity analysis
A local sensitivity assessment was performed to quantify how model parameters influence UCMR. Each parameter (pi) was perturbed ±10% from its baseline value (Pi,0), producing Pi,−Δ and Pi,+Δ. The impact on the 8-hour UCMR output (q) was recorded. Sensitivity S(q, pi, AS) was computed across a set of activity scores (0, 0.25, 0.5, 1, 1.25, 1.5, 2.0, 3.0) using the prescribed formula.

$$S(q, pi, AS) = \frac{1}{2} \cdot \frac{q(Pi, -\Delta, AS) - q(Pi, -\Delta, AS)}{Pi, 0} \tag{2}$$

Results and Discussion

In this study, a physiologically based pharmacokinetic (PBPK) framework for DXM was created and used to analyze how CYP2D6 genetic variability influences DXM disposition and phenotype classification derived from DXM metabolism.

Pharmacokinetics database of DXM
To build and assess the model, an extensive dataset covering DXM and its metabolites was assembled from 36 human studies **(Table 1)**. Most investigations focused on drug–gene interactions (DGI), drug–drug interactions (DDI), or combined drug–drug–gene interactions. Nearly all trials used oral DXM dosing (n = 35), while only one study administered the compound intravenously (n = 1) [50]. Formulations differed substantially between reports (solution, syrup, capsules, tablets), as did dosing ranges (2 mg–3 mg/kg), co-medications (phenotyping cocktails, quinidine, cinacalcet hydrochloride, zuojin), sampling schedules, and biological matrices (urine, plasma, serum).

A key strength of this compilation is the inclusion of numerous individual UCMR values accompanied by CYP2D6 genotype information (11 studies). To our knowledge, this represents the first broad, openly available DXM pharmacokinetic collection, hosted in the PK-DB database [38].

PBPK model of DXM
A PBPK model **(Figure 1)** was constructed to examine CYP2D6 polymorphism effects on DXM kinetics and DXM-based metabolic phenotyping. **Table 2** lists the essential parameters. The model utilizes a hierarchical design: at the whole-body level **(Figure 1a)**, compartments include liver, kidneys, intestine, forearm, lung, and a residual compartment aggregating remaining tissues. All compartments are linked via systemic blood flow. DXM can be introduced intravenously (IV) or orally (PO), entering either the venous circulation or the intestinal lumen. The intestinal component **(Figure 1b)** captures dissolution, uptake, and loss of DXM; only part of the dose is absorbed, with the rest eliminated in feces. DXM crosses enterocytes into the blood, where intestinal CYP3A4 contributes to first-pass N-demethylation, decreasing the amount reaching systemic circulation.

Within the hepatic module **(Figure 1c)**, DXM undergoes O-demethylation to DXO and subsequent conjugation to DXO-Glu. These steps follow Michaelis–Menten kinetics defined by Km and Vmax. O-demethylation is mediated by both CYP3A4 and CYP2D6, with CYP2D6 kinetic constants modulated by activity score (AS) as described in Section 3.3.

The renal subsystem **(Figure 1d)** represents the urinary elimination of DXM, DXO, and DXO-Glu.

Table 2. details the PBPK model's parameters; prefixes GU__, LI__, and KI__ indicate gut, liver, and kidney parameters. Values originate from literature or fitting (F). Some parameters were scanned (S), and local sensitivity analyses (SA) are summarized in Section 3.5.

Parameter	Description	Reference(s)	Value	Unit	Fixed (F)	Sensitivity (S)	Scenario analysis (SA)
BW	Body weight (adult male)	ICRP (2002) [86]	75	kg	✓		
Height	Body height (adult male)	ICRP (2002) [86]	170	cm	✓		
HR	Heart rate	ICRP (2002) [86]	70	min⁻¹	✓		
HRrest	Resting heart rate	ICRP (2002) [86]	70	min⁻¹	✓		
COBW	Cardiac output per kg body weight	ICRP (2002); de Simone *et al.* (1997) [86, 87]	1.548	mL/s/kg	✓	✓	
HCT	Hematocrit (upper male range)	Vander (2001); Herman (2016) [88, 89]	0.51	–		✓	
Kp_fo_dxm	Forearm tissue/plasma partition coefficient (dextromethorphan)	Calculated	10	–		✓	✓
f_shunting_forearm	Fractional shunting in forearm	Literature	0.27975	–		✓	
FVgu	Gut fractional organ volume	Jones and Rowland-Yeo (2013); ICRP (2002) [86, 90]	0.0171	L/kg	✓		
FVki	Kidney fractional organ volume	Jones and Rowland-Yeo (2013); ICRP (2002) [86, 90]	0.0044	L/kg	✓		
FVli	Liver fractional organ volume	Jones and Rowland-Yeo (2013); ICRP (2002) [86, 90]	0.021	L/kg	✓	✓	
FVlu	Lung fractional organ volume	Jones and Rowland-Yeo (2013); ICRP (2002) [86, 90]	0.0076	L/kg	✓		
FVsp	Spleen fractional organ volume	Jones and Rowland-Yeo (2013); ICRP (2002) [86, 90]	0.0026	L/kg	✓		
FVpa	Pancreas fractional organ volume	Jones and Rowland-Yeo (2013); ICRP (2002) [86, 90]	0.01	L/kg	✓		
FVfo	Forearm fractional organ volume	Jones and Rowland-Yeo (2013); ICRP (2002) [86, 90]	0.0048	L/kg	✓	✓	
FVve	Venous blood fractional volume	Jones and Rowland-Yeo (2013); ICRP (2002) [86, 90]	0.0514	L/kg	✓		
FVar	Arterial blood fractional volume	Jones and Rowland-Yeo (2013); ICRP (2002) [86, 90]	0.0257	L/kg	✓		
FVpo	Portal vein fractional volume	Jones and Rowland-Yeo (2013); ICRP (2002) [86, 90]	0.001	L/kg	✓		
RQgu	Fractional blood flow to gut	Jones and Rowland-Yeo (2013) [90]	0.146	–		✓	
RQki	Fractional blood flow to kidney	Jones and Rowland-Yeo (2013) [90]	0.19	–		✓	
RQh	Fractional hepatic venous blood flow	Jones and Rowland-Yeo (2013) [90]	0.215	–		✓	

Parameter	Description	Reference	Value	Unit			
RQlu	Fractional blood flow to lung	Jones and Rowland-Yeo (2013) [90]	1.0	–			✓
RQsp	Fractional blood flow to spleen	Jones and Rowland-Yeo (2013) [90]	0.017	–			✓
RQfo	Fractional blood flow to forearm	RNAO (2022) [91]	0.0146	–			✓
RQpa	Fractional blood flow to pancreas	ICRP (2002) [86]	0.017	–			✓
tissue_dxm_Vmax	Maximum velocity of non-specific tissue distribution (DXM)	Fitted	1000	L/min		✓	✓
Kp_dxm	Global tissue/plasma partition coefficient (DXM)	Calculated/fitted	8.7346	–		✓	✓
Ka_diss_dxm	First-order rate of dissolution and gastric emptying (DXM)	CHEBI:29133	0.0217	h⁻¹		✓	✓
MW_dxo	Molecular weight of dextrorphan (DXO)	CHEBI:29133	257.3707	g/mol	✓		
tissue_dxo_Vmax	Maximum velocity of non-specific tissue distribution (DXO)	Fitted	100	L/min		✓	✓
Kp_dxo	Tissue/plasma partition coefficient (DXO)	Calculated	4	–		✓	✓
MW_dxo_glu	Molecular weight of dextrorphan O-glucuronide	CHEBI:32645	433.4998	g/mol	✓		
tissue_dxo_glu_Vmax	Maximum velocity of non-specific tissue distribution (DXO-Glu)	Fitted	3	L/min		✓	✓
Kp_dxo_glu	Tissue/plasma partition coefficient (DXO-Glu)	Calculated	0.8	–		✓	✓
KI_DXMEXE_k	First-order urinary excretion rate constant (DXM)	Fitted	0.017	min⁻¹		✓	✓
KI_DXOEXE_k	First-order urinary excretion rate constant (DXO)	Literature/fitted	0.3	min⁻¹		✓	✓
KI_DXOGLUEX_k	First-order urinary excretion rate constant (DXO-Glu)	Fitted	10	min⁻¹		✓	✓
LI_DXMCYP2D6_Vmax	Hepatic CYP2D6 Vmax for dextrorphan formation	Fitted	0.003	mmol/min/L		✓	✓
LI_DXMCYP2D6_Km	Hepatic CYP2D6 Km (DXM)	Storelli *et al.* (2019a); Yang *et al.* (2012) [84, 85]	0.0079	mM	✓		
LI_cyp2d6_ac	CYP2D6 activity score	Storelli *et al.* (2019a); Yang *et al.* (2012) [84, 85]	0.0 – 3.0	–			✓
LI_lambda_1	Slope of principal component regression (Km vs Vmax in log space)	Storelli *et al.* (2019a); Yang *et al.* (2012) [84, 85]	–0.4	–			✓
LI_DXMCYP3A4_Vmax	Hepatic CYP3A4 Vmax for dextrorphan formation	Fitted	0.0004	mmol/min/L		✓	✓
LI_DXMCYP	Hepatic CYP3A4 Km (DXM → DXO)	Yu and Haining (2001)[35]	0.157	mM	✓		

3A4_K m						
LI_DX OUGT_ Vmax	Hepatic UGT Vmax for DXO glucuronidation	Lutz and Isoherranen (2012) [30]	0.8953	mmol/ min/L		✓ ✓
LI_DX OUGT_ Km	Hepatic UGT Km for DXO glucuronidation	Lutz and Isoherranen (2012) [30]	0.69	mM	✓	
GU_F_ dxm	Fraction of DXM absorbed from gut	Schadel *et al.* (1995) [26]	0.55	–		✓
GU_Ka _abs_d xm	First-order absorption rate constant (DXM)	Schadel *et al.* (1995) [26]	3.4285	h⁻¹		✓ ✓
GU_D XMCY P3A4_ Vmax	Intestinal CYP3A4 Vmax (DXM metabolism)	Kerry *et al.* (1994); Yu and Haining (2001) [35, 92]	0.0002	mmol/ min/L		✓ ✓
GU_D XMCY P3A4_ Km	Intestinal CYP3A4 Km (DXM)	Kerry *et al.* (1994); Yu and Haining (2001) [35, 92]	0.7	mM	✓	
PODOS E	Oral dextromethorphan dose	Variable	–	mg		✓ ✓

This model predicts DXM, DXO, and DXO-Glu concentrations and quantities as functions of CYP2D6 genotype, diplotype, and AS, with outputs evaluated in urine or plasma (median cubital vein). To our knowledge, this is the first publicly accessible, reusable DXM PBPK model, distributed in SBML format at: https://github.com/matthiaskoenig/dextromethorphan-model.

CYP3A4 and CYP2D6 variability

Cytochrome P450 enzymes show marked person-to-person variation. To represent this, a stochastic model describing CYP2D6 and CYP3A4 activities was formulated using bivariate lognormal distributions for Km and Vmax, fitted to human liver microsome measurements [84, 85] **(Figure 2)**.

For CYP2D6, Vmax was modeled as directly proportional to the AS, with AS = 0 representing the absence of CYP2D6 function. The spread of Km and Vmax was assumed uniform across AS categories. Mixture weights P(AS) were derived from a curated dataset describing observed activity-score frequencies and UCMR distributions. Increasing AS results in higher maximal catalytic rates (Vmax) for DXM O-demethylation and improved substrate affinity (lower Km). Although the CYP3A4 and CYP2D6 models match reported experimental data, limited genotype detail restricts the validation of AS-specific predictions. As noted earlier, individuals with no functional CYP2D6 alleles still generate small quantities of DXO. This was captured by incorporating a secondary CYP3A4-mediated O-demethylation route, adopting the mean DXM Km reported by Yu and Haining (2001) [35]. Variability in Km and Vmax for this pathway was assumed equivalent to the midazolam-derived CYP3A4 estimates from Storelli *et al.* (2019a) and Yang *et al.* (2012) [84, 85]. Integrating this enzyme-variability component with the PBPK model enabled simulation of (i) the impact of CYP parameter diversity on DXM kinetics and (ii) the consequences of AS on CYP2D6 function and overall DXM pharmacokinetics.

Influence of the CYP2D6 activity score on DXM pharmacokinetics

To examine model behavior, predicted profiles were compared visually with standard pharmacokinetic readouts— DXM, DXO, plasma DXM/DXO, and urinary DXM/(DXO + DXO-Glu)—for individuals with known activity scores (AS) or diplotypes **(Figure 3)**. For every AS category, a virtual cohort of 2,000 parameter sets (Km and Vmax) was generated from the stochastic CYP3A4/CYP2D6 models. Each AS group was simulated with a 30 mg oral DXM dose and matched against corresponding observations. The model reproduces the pronounced within-AS and between-AS variability. As AS rises and CYP2D6 activity increases, plasma DXM declines **(Figure 3a)**, plasma DXO rises **(Figure 3b)**, and the DXM/DXO ratio falls **(Figure 3c)**, consistent with earlier reports [40, 45]. The broad dispersion within an AS group reflects the large inherent spread in CYP2D6 kinetic parameters

(Figure 2). Substantial overlap between adjacent AS distributions leads to overlapping pharmacokinetic behavior across neighboring groups.
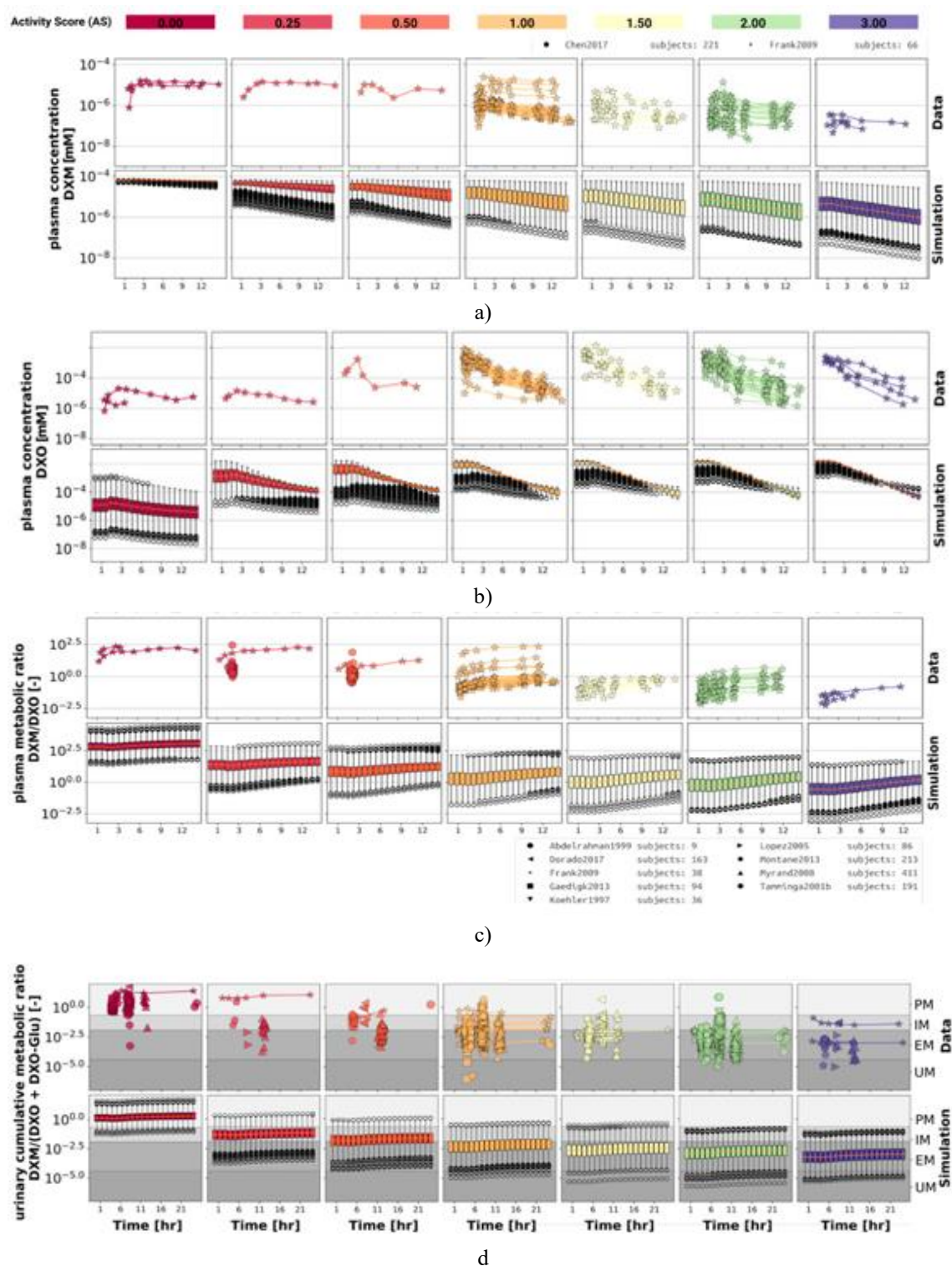

Figure 3. Time profiles of DXM kinetics stratified by AS. Panels show: (a) DXM concentration, (b) DXO concentration, (c) DXM/DXO plasma ratio, (d) UCMR (urinary DXM/(DXO + DXO-Glu)). Only datasets involving 30 mg oral DXM are shown in A–C. The upper rows display data from healthy subjects [40, 41, 45, 48, 55, 59, 60, 62, 63, 70]. Cocktail studies were retained, but trials using known interacting co-medications were removed. The lower rows show simulations. Box plots present quartiles, medians, and outliers for selected time points. CYP3A4/CYP2D6 Km and Vmax values follow the distributions in **Figure 2**, and the corresponding AS-specific CYP2D6 models were applied.

The UCMR **(Figure 3d)** remains essentially constant over time, aligning well with measurements. UCMR decreases steadily with higher AS, shifting subjects along the PM→IM→EM phenotype spectrum. Unlike A–C, the UCMR dataset was pooled irrespective of DXM dose because the metric is dose-insensitive (Section 3.5). Overall, despite limited time-course information for very low AS groups (0, 0.25, 0.5), the model captures AS-dependent DXM behavior accurately.

To further assess predictive quality, simulations were matched with datasets for plasma/serum DXM **(Figure 4)**, plasma/serum DXO **(Figure 5)**, plasma/serum total DXO (DXO + DXO-Glu) **(Figure 6)**, urinary DXM **(Figure 7)**, urinary total DXO **(Figure 8)**, and UCMR **(Figure 9)**. Given the expected variability, the model reproduced all datasets satisfactorily, with a mild tendency to predict slightly faster kinetics for plasma DXO + DXO-Glu **(Figure 6)**.
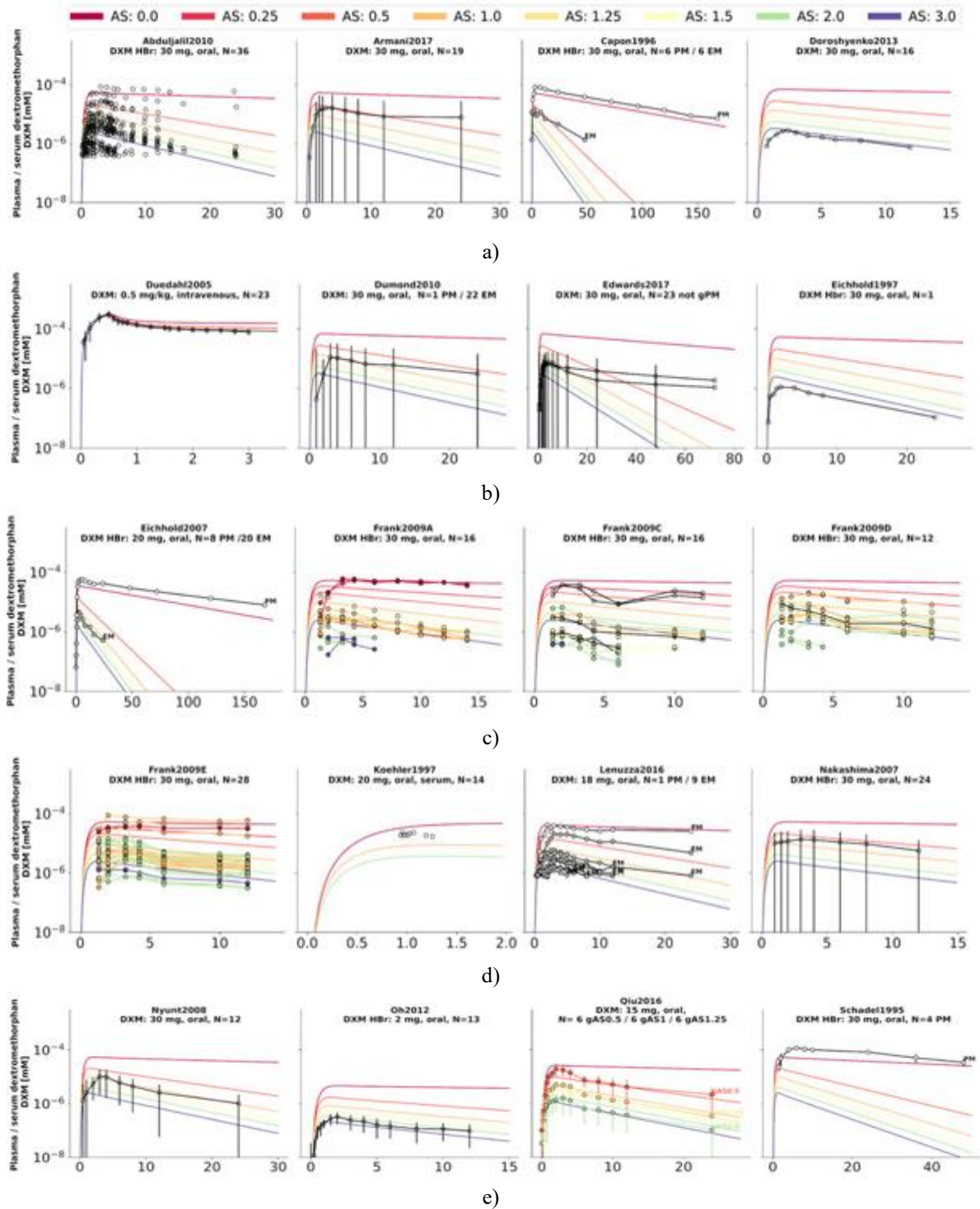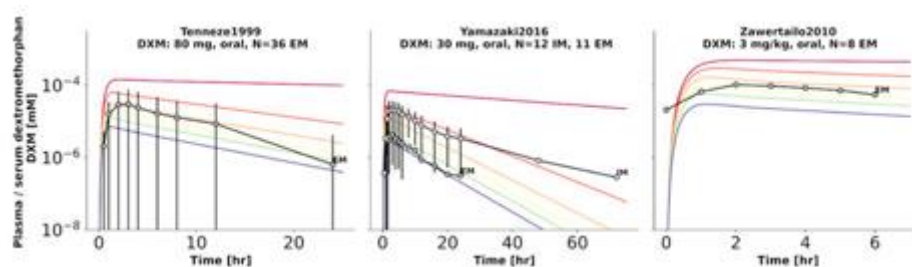
f)

Figure 4. Plasma/serum DXM concentrations. Protocols were simulated using the reported doses. When AS values were provided, data points were color-coded. Phenotype labels (UM, EM, IM, PM) are shown where available. Data from: Schadel *et al.*, 1995; Capon *et al.*, 1996; Eichhold *et al.*, 1997, 2007; Köhler *et al.*, 1997; Tennezé *et al.*, 1999; Duedahl *et al.*, 2005; Nakashima *et al.*, 2007; Nyunt *et al.*, 2008; Frank, 2009; Abduljalil *et al.*, 2010; Dumond *et al.*, 2010; Zawertailo *et al.*, 2010; Oh *et al.*, 2012; Doroshyenko *et al.*, 2013; Lenuzza *et al.*, 2016; Qiu *et al.*, 2016; Armani *et al.*, 2017; Edwards *et al.*, 2017; Yamazaki *et al.*, 2017 [26–28, 43, 49, 50, 52–54, 59, 61, 67, 68, 71, 72].
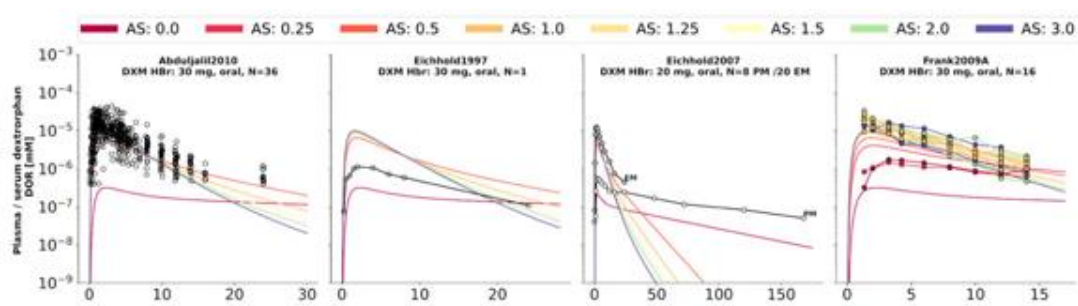
a)
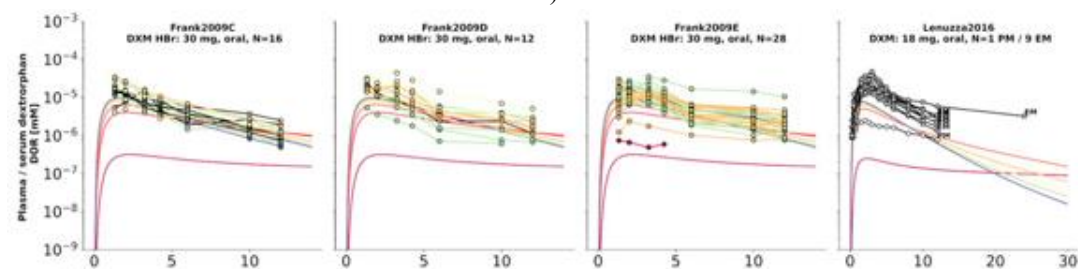
b)
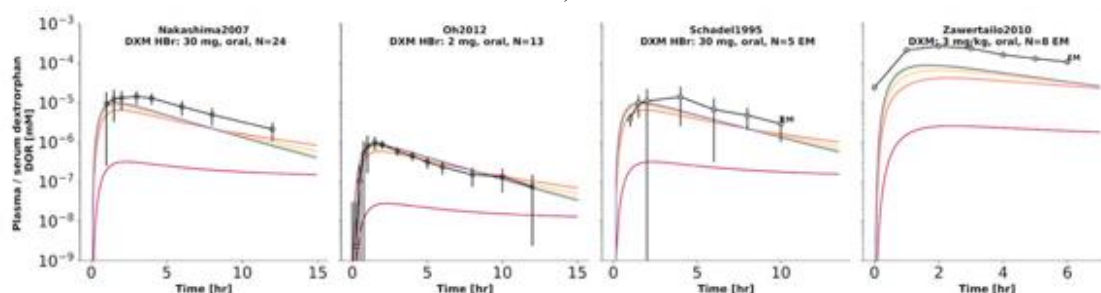
c)

Figure 5. Plasma/serum DXO concentrations. Studies were simulated per their dosing instructions. AS/phenotype color-coding is included when reported. Data from: Schadel *et al.*, 1995; Eichhold *et al.*, 1997, 2007; Nakashima *et al.*, 2007; Frank, 2009; Abduljalil *et al.*, 2010; Zawertailo *et al.*, 2010; Oh *et al.*, 2012; Lenuzza *et al.*, 2016.
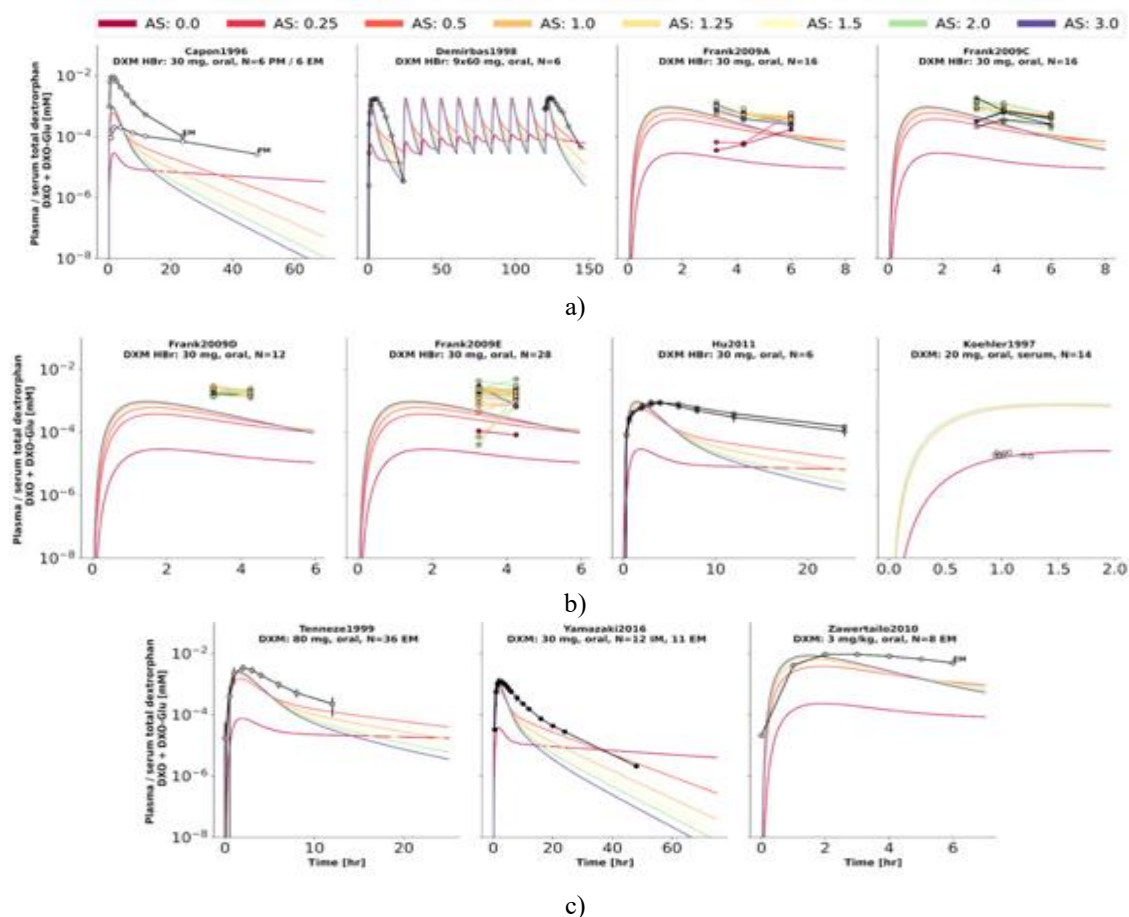
Figure 6. Plasma/serum total DXO (DXO + DXO-Glu). Simulations followed the documented dosing schemes. Phenotype and AS color-coding are shown where reported. Data from: Capon *et al.*, 1996; Köhler *et al.*, 1997; Demirbas *et al.*, 1998; Tennezé *et al.*, 1999; Zawertailo *et al.*, 2010; Hu *et al.*, 2011; Yamazaki *et al.*, 2017 [26, 28, 47, 57, 59, 71, 72].
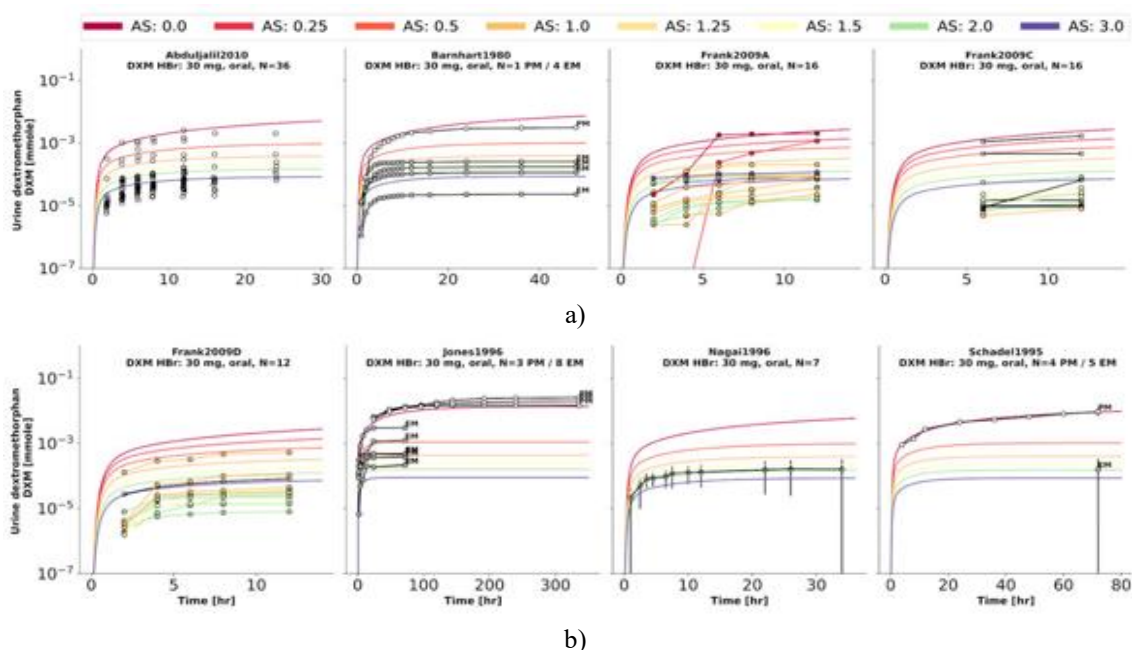

Figure 7. Urinary DXM amounts. Simulations were carried out following each study's dosing schedule. Phenotype categories were added where available. Data from: Barnhart, 1980; Schadel *et al.*, 1995; Jones *et al.*, 1996; Nagai *et al.*, 1996; Frank, 2009; Abduljalil *et al.*, 2010.
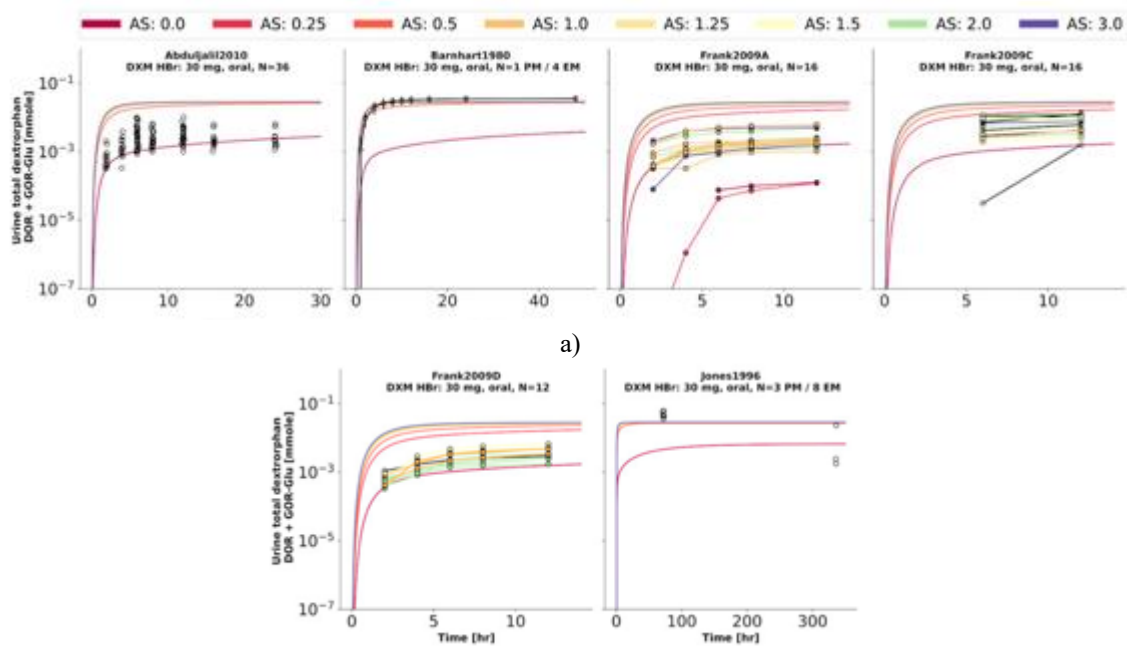
Figure 8. Urinary total DXO (DXO + DXO-Glu). Simulations matched the original dosing protocols.
Phenotype groups are indicated where reported. Data from: Barnhart, 1980; Jones *et al.*, 1996; Frank, 2009;
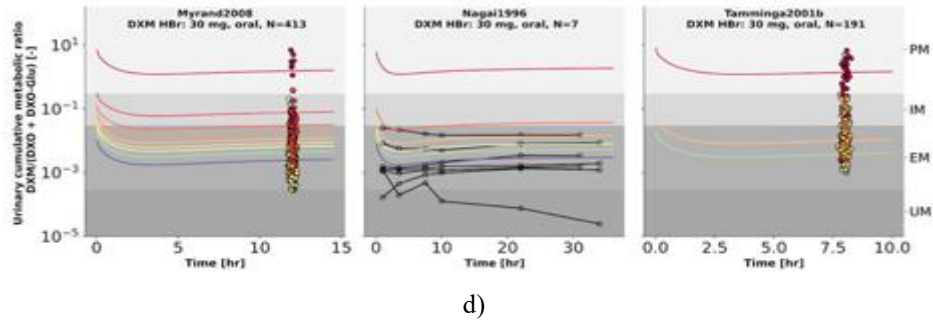Abduljalil *et al.*, 2010 [40, 42, 44, 58].

d)
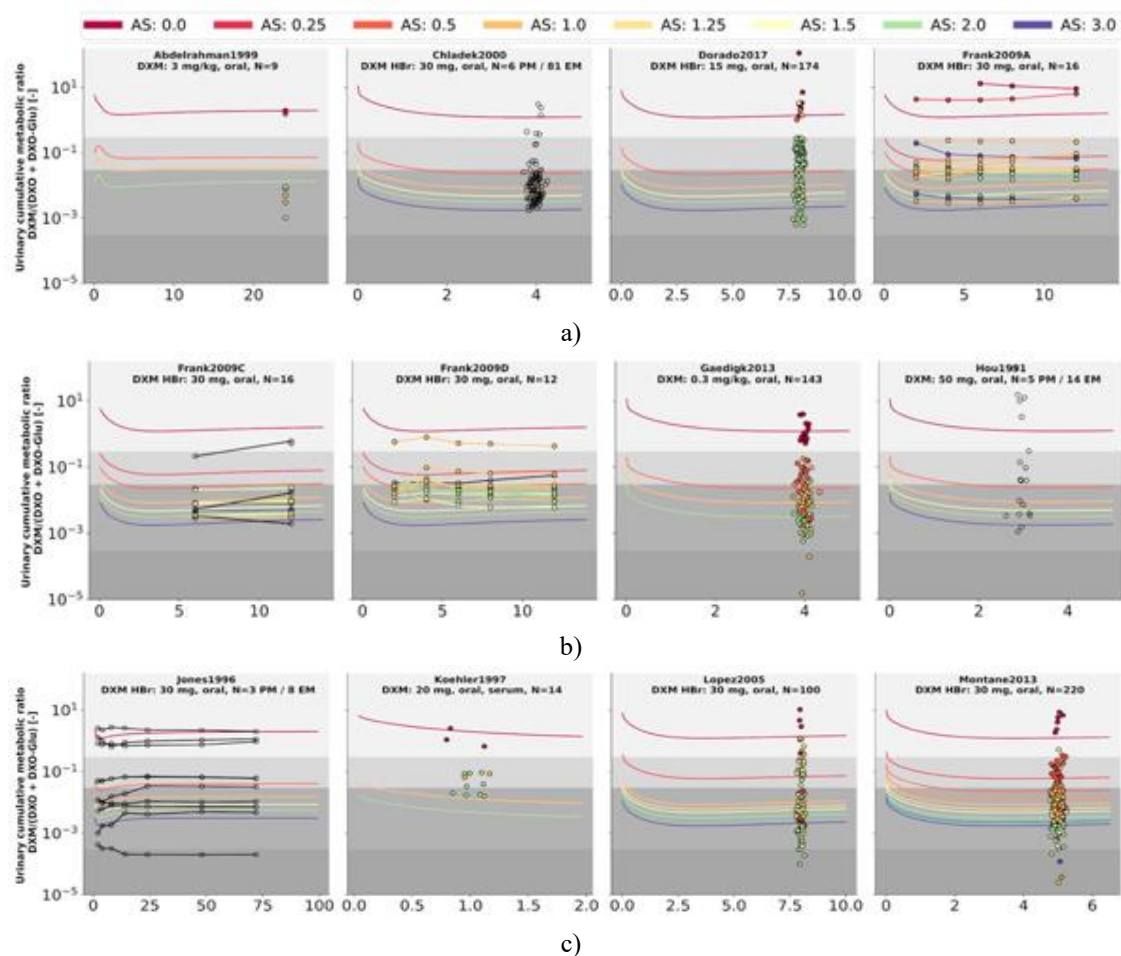
Figure 9. Urinary cumulative metabolic ratio of dextromethorphan to total dextrorphan, DXM/(DXO + DXO-Glu) (UCMR). Each study was simulated using its original dosing scheme. When activity-score data were available, the corresponding clinical points were color-labeled; reported metabolizer classes (UM, EM, IM, PM) are shown as indicated. Data originate from Hou *et al.* (1991); Jones *et al.* (1996); Nagai *et al.* (1996); Köhler *et al.* (1997); Abdelrahman *et al.* (1999); Chládek *et al.* (2000); Tamminga *et al.* (2001); López *et al.* (2005); Myrand *et al.* (2008); Frank (2009); Gaedigk (2013); Montané Jaime *et al.* (2013); Dorado *et al.* (2017) [40, 41, 46, 48, 55, 56, 58–60, 62–64, 70]. The phenotype boundaries for UM, EM, IM, and PM are illustrated as shaded regions.

Influence of parameters on phenotyping using UCMR

Determining how parameter variation alters UCMR is important for recognizing sources of bias or misclassification in UCMR-based phenotype assignment. A central question is whether these influences differ across CYP2D6 activity scores.

To assess this, several physiological and dosing-related variables—liver size, cardiac output, the tissue-to-plasma partition coefficient of DXM, and the administered oral dose—were adjusted within plausible limits, and the resulting UCMR at 8 h after a 30-mg DXM dose was evaluated **(Figure 10a)**. Regardless of activity score, UCMR rose with larger liver volume and declined when cardiac output was increased. Changing DXM partitioning or the oral amount of DXM produced only minor shifts in UCMR.
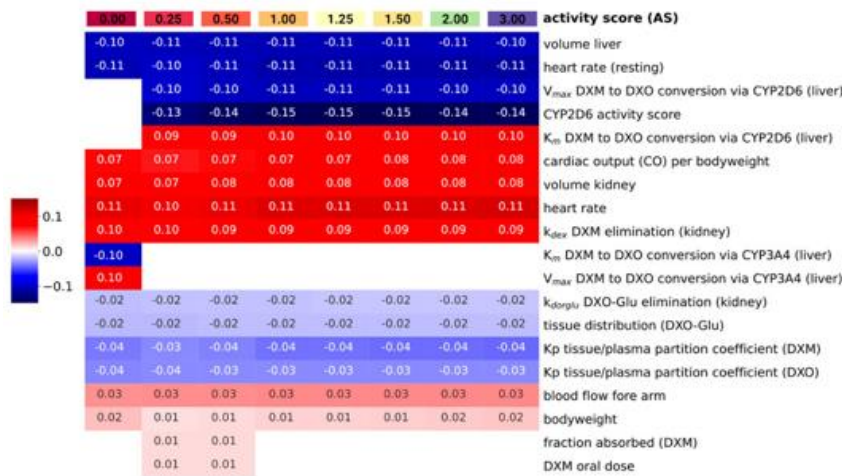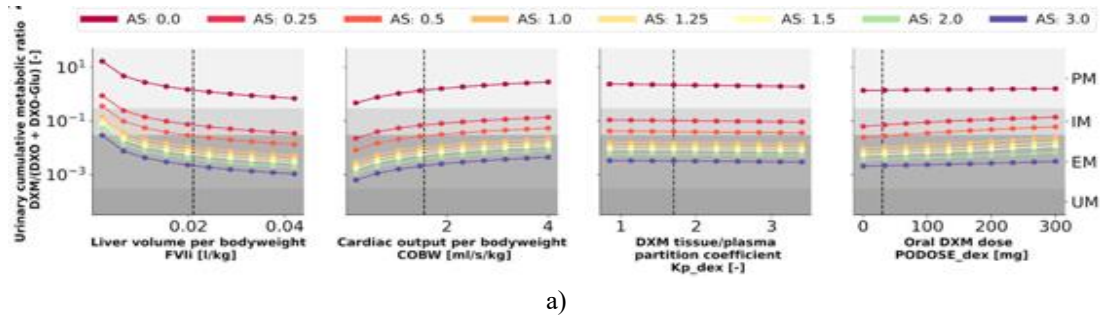

a)

b)

Figure 10. Sensitivity of UCMR across activity scores.

(a) Relationship between UCMR (DXM/(DXO-Glu) at 8 h after 30 mg DXM and selected physiological variables and dose. Parameter sweeps were performed for all activity scores. Baseline values are represented by dashed lines.

(b) Parameter-level sensitivity analysis. Local sensitivities of UCMR were calculated for every activity score by perturbing each parameter by ±10% around its reference value. Parameters causing <1% relative UCMR change were excluded. Positive effects are shown in red and negative effects in blue. Parameters were grouped by agglomerative clustering. Representative parameters from these clusters (liver volume per body weight, cardiac output per body weight, DXM tissue/plasma partitioning, and oral dose) correspond to those illustrated in (a). Sensitivity values in (b) reflect the normalized local slope at the dashed lines in (a).

The modeling results indicate that UCMR remains stable over time **(3D and Figure 9)** and is largely unaffected by differences in dosing procedures (e.g., amount of DXM, dissolution kinetics). UCMR also shows moderate resilience to physiological variability **(Figure 10b)**. Changes in liver size, heart rate, cardiac output, kidney size, and renal clearance of DXM influence UCMR to a degree comparable to CYP2D6 kinetic parameters, although natural biological variability in these physiological factors is far smaller. No sensitivity to UGT Vmax or Km was detected, providing the rationale for not exploring inter-individual UGT variability further.

For most parameters, local sensitivities were nearly identical across activity scores, meaning that physiological influences were proportionally similar at all AS levels. For AS = 0, the assumption of limited CYP3A4-mediated DXM metabolism shifts control of UCMR away from CYP2D6 and toward CYP3A4. Even with heterogeneous study protocols, UCMR appears to be a generally reliable—though not flawless—indicator for comparing CYP2D6 function. The analysis suggests that UCMR values from different studies can be combined **(Figure 3d)**, although methodological differences may still introduce some error.

Impact of CYP2D6 variants and activity score on UCMR
We next evaluated whether the model accurately reproduces UCMR distributions for specific CYP2D6 genotypes and activity scores **(Figure 11)**. Predicted distributions derived from genotype frequencies were contrasted with observed datasets. For each AS category, the model reproduced the general shape and position of the UCMR distributions. Higher activity scores corresponded to lower UCMR values, yet substantial overlap between AS groups was present, consistent with the broad CYP2D6 parameter variability across scores. Model-generated distributions were slightly narrower than clinical data, potentially due to unmodeled physiological variation, unaccounted UGT diversity, genotype-assignment uncertainties, unidentified modifiers, or study-level biases.
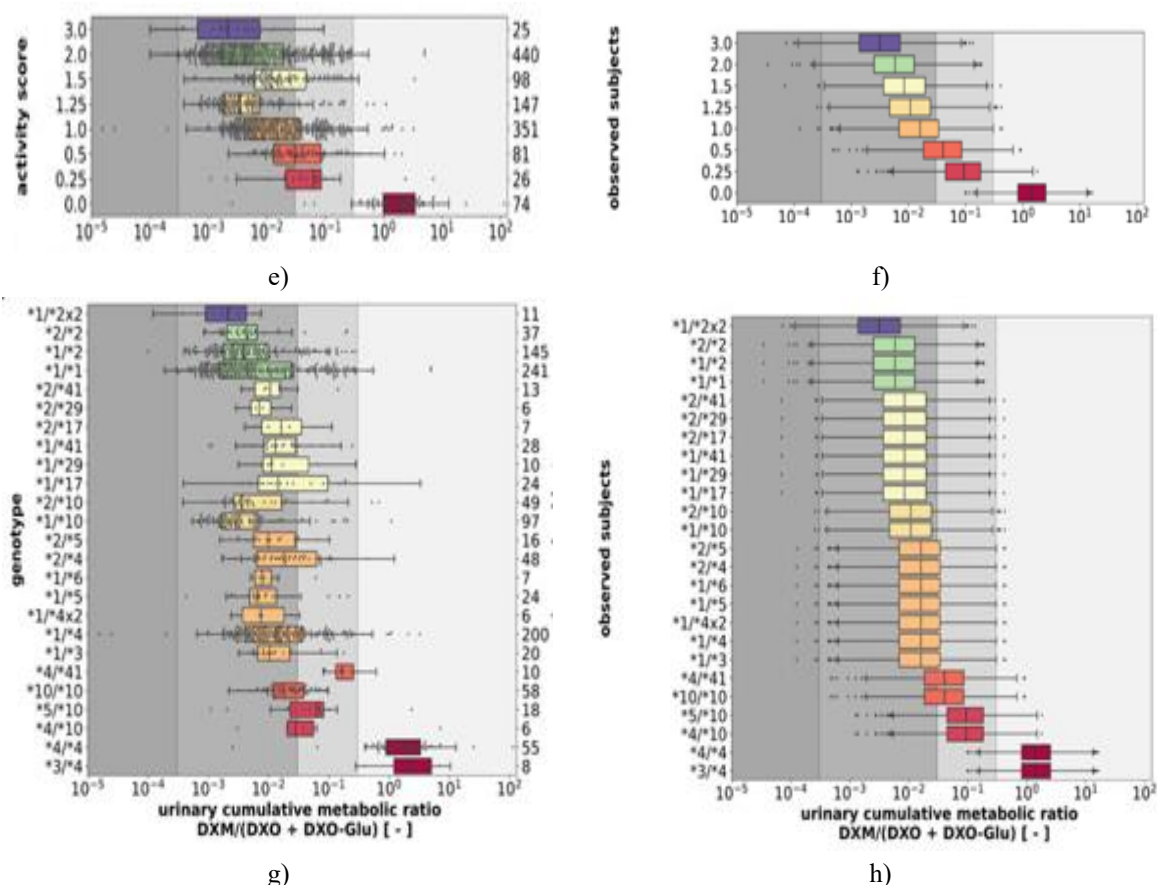
e)

f)

g)

h)
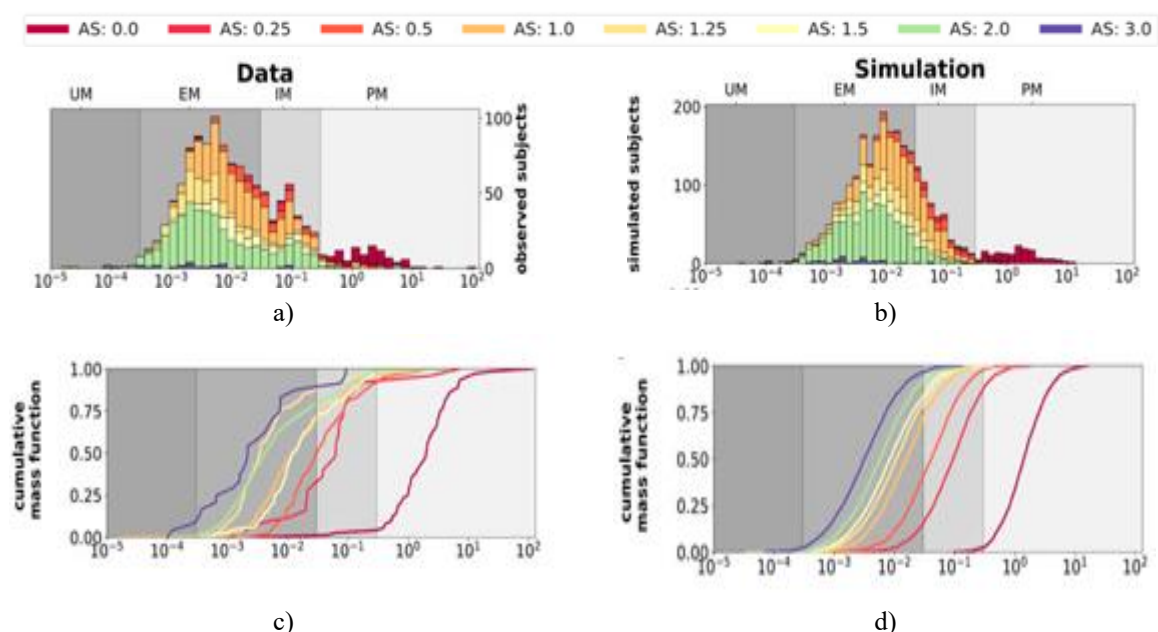
Figure 11. Relationship between CYP2D6 genotype, activity score, and the urinary cumulative ratio DXM/(DXO-Glu) (UCMR). The figure shows simulations based on activity-score distributions. All UCMR measurements were taken ≥4 h after administration of DXM hydrobromide in healthy adult volunteers. Studies involving phenotyping cocktails were retained, but those with known drug–drug interactions were removed. Gray zones indicate the activity-based phenotype categories (UM, EM, IM, PM). For time-dependent datasets, only the final post-dose UCMR point was analyzed. Data sources: Köhler *et al.* (1997); Abdelrahman *et al.* (1999); Tamminga *et al.* (2001); López *et al.* (2005); Myrand *et al.* (2008); Frank (2009); Gaedigk (2013); Montané Jaime *et al.* (2013); Dorado *et al.* (2017) [40, 41, 48, 55, 59, 60, 62, 63, 70]. (a) Histograms of observed UCMR values grouped by activity score. (b) Matching model output (UCMR at 8 h) generated via Monte Carlo simulation using Km and Vmax as stochastic variables **(Figure 2)**. (c) Empirical cumulative mass functions (CMFs) arranged by activity score. (d) Simulated CMFs for the same activity-score groups. (e) Box-and-whisker plots of recorded UCMRs by activity score. (f) Equivalent box plots of simulated values. (g) Observed UCMRs grouped by CYP2D6 diplotype. (h) Simulated UCMRs grouped by diplotype. For panels d, f, and h, 2,000 samples were generated per activity score; panels b and d include an additional two-fold oversampling reflecting activity-score frequencies in the empirical dataset.

The activity-score framework could be made more precise. Treating CYP2D6 genotypes as fixed stepwise categories (0, 0.25, 0.5, 1) oversimplifies the spectrum of enzyme activity; a continuous scale would likely capture the variation more accurately. Both the model output and available data show that gUM individuals (AS ≥ 3) cannot reliably be classified as ultrarapid metabolizers, whereas gPMs (AS = 0) remain the only group that can be consistently separated from the rest **(Figures 11c–11f)**. A notable advantage of the current modeling strategy is its ability to infer in vivo metabolic behavior directly from in vitro kinetic inputs.

Variability in UCMR across global populations
The model was also used to forecast UCMR distributions for different biogeographic groups **(Figure 12)** using population-specific activity-score frequencies. Simulations were run for 30 mg DXM at 8 h post-dose for populations from Oceania, the Near East, the Americas, Latino groups, Central/South Asia, African American/Afro-Caribbean regions, Sub-Saharan Africa, Europe, and East Asia **(Figure 12a)**. Observed UCMRs

for Caucasian and East Asian groups **(Figure 12b)** were compared with the simulations **(Figure 12c)**. The predicted values match well with published measurements for these populations [40, 41, 55, 59, 63].
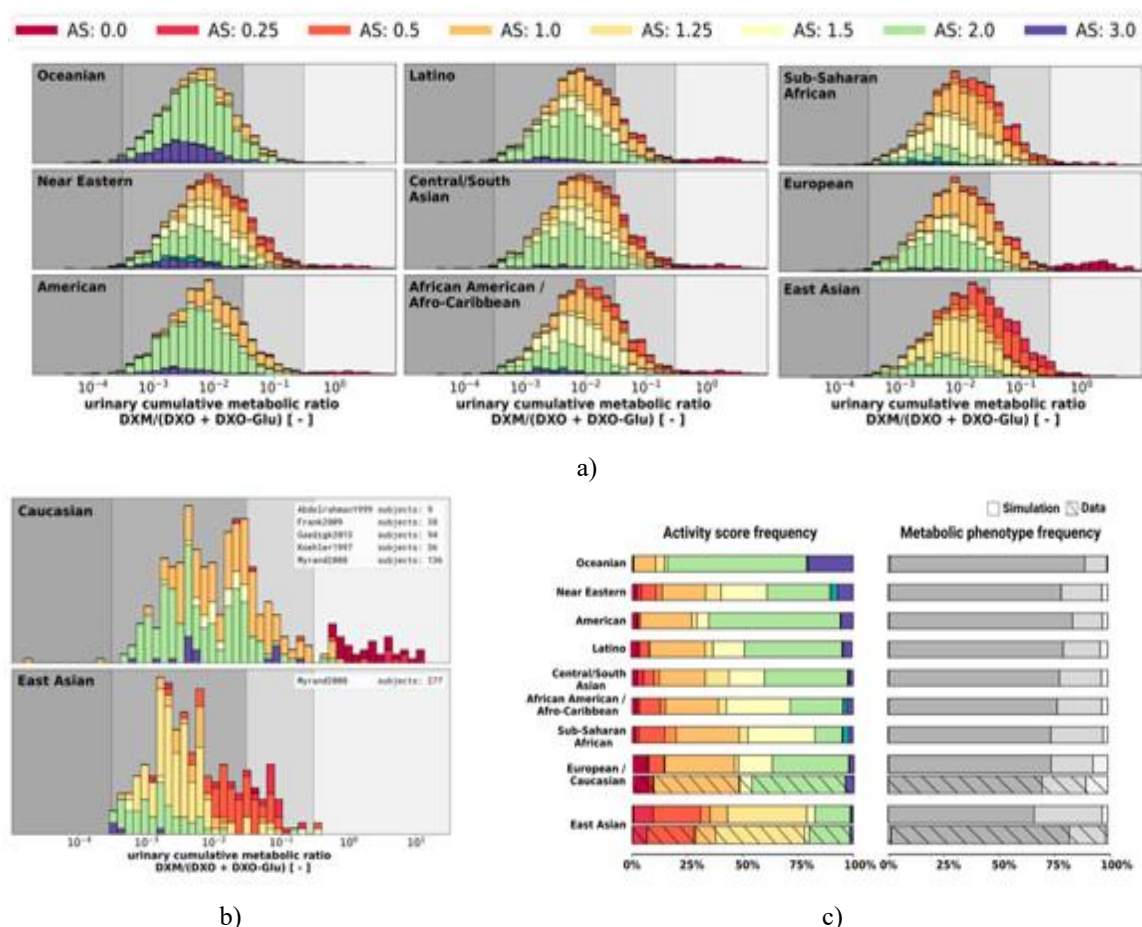

Figure 12. UCMR distributions by population.
(a) Model-generated UCMR distributions at 8 h for several biogeographical groups using CYP2D6 activity-score frequencies from PharmGKB [21]. (b) Published UCMR measurements for Caucasian and East Asian subjects, grouped by activity score [40, 41, 55, 59, 63]. Cocktail studies were retained; trials involving known drug–drug interactions were excluded. (c) Simulated AS and phenotype frequencies for the populations and comparison with the available Caucasian and East Asian datasets (hatched columns).

Over the past two decades, a wide range of modeling platforms—GastroPlus [93], P-Pharm [94], SAS [95, 96], SimCYP [97–104], MATLAB [105], and PK-Sim [106]—have been used to explore DXM pharmacokinetics. Yet many published models cannot be externally validated or integrated into new work due to restricted availability, missing model files, or platform-specific limitations. Here, we provide a fully accessible, reproducible, and platform-independent whole-body representation of DXM disposition, enabling transparent reuse, comparison, and future expansion.

In addition, modeling efforts that aim for strong empirical grounding require reliable supporting data. Broader, independent datasets enhance the robustness of conclusions. Practices used in systematic reviews, such as PRISMA guidelines for transparent reporting, were adapted where feasible for selecting and evaluating literature sources for the present analysis. This approach helped identify and reduce sources of bias. Crucially, our open model is complemented by a large, openly available pharmacokinetic database.

The PBPK framework presented here can forecast dextromethorphan (DXM) biotransformation at both population and individual levels using CYP2D6 genotypic information. To our knowledge, it is the first model able to estimate personal UCMR values as well as the overall distribution of UCMRs. It also captures a wide spectrum of published clinical observations for DXM and provides clearer insight into how DXM pharmacokinetics should be interpreted. Notably, the results indicate that CYP2D6 function is not the sole factor shaping UCMR, which is evident from the substantial variability and overlap in activity scores. Thus, UCMR should be used cautiously as

a surrogate for CYP2D6 phenotypes. The simulations further demonstrate that when CYP2D6 activity is extremely low, UCMR is influenced predominantly by processes other than CYP2D6 itself—aligning with prior findings showing that CYP2D6 inhibition mainly affects poor metabolizers [36].

Although the current implementation already provides considerable utility, there remains substantial potential for refinement. By releasing both data and model in open, standardized formats, we aim to support future expansions and revisions by the community.

A number of physiological inputs had to be inferred or fitted despite being theoretically measurable. For example, the unexpectedly low plasma concentrations of DXM imply notable extravascular binding. Yet, obtaining reliable tissue-plasma partition coefficients (Kp) is challenging, and available evidence is sparse. Steinberg *et al.* (1996) [107] documented roughly 68-fold higher levels in brain tissue and about 4-fold lower levels in cerebrospinal fluid compared to serum. Other groups have proposed Kp ≈ 1.65 based on n-octanol/water partitioning, while additional mechanisms such as lysosomal sequestration have also been proposed [93]. In our simplified model—where tissue distribution uses uniform Kp and ftissue values—the kinetics of DXO-Glu appear somewhat too fast **(Figure 6)**. This likely stems from the reduced structural complexity. In general, glucuronide conjugates differ markedly from their parent molecules in polarity, plasma-protein binding, lipid solubility, renal elimination, and tissue uptake.

A major bottleneck in further refining the model is the scarcity of experimental data linking CYP2D6 genotype with enzyme activity. Only a few studies offer such measurements [85, 108, 109]. Moreover, no study has reported parallel in vitro activity and UCMR measurements—both of which would be critical for validating the activity score (AS) system and developing models that incorporate genetic structural variation [109]. For example, the AS framework alone cannot account for genotype-dependent differences in the extent of CYP2D6 inhibition [68].

Conclusion

In summary, we constructed and validated a PBPK model for DXM and used it to investigate how CYP2D6 genetic diversity shapes metabolic phenotyping outcomes.

References

1. Saravanakumar A, Sadighi A, Ryu R, Akhlaghi F. Physicochemical properties, biotransformation, and transport pathways of established and newly approved medications: A systematic review of the top 200 most prescribed drugs vs the FDA-approved drugs between 2005 and 2016. Clin Pharmacokinet. 2019;58(10):1281–94. doi:10.1007/s40262-019-00750-8

2. Hurtado I, García-Sempere A, Peiró S, Sanfélix-Gimeno G. Increasing trends in opioid use from 2010 to 2018 in the region of Valencia, Spain: A real-world, population-based study. Front Pharmacol. 2020;11(1):612556. doi:10.3389/fphar.2020.612556

3. Kibaly C, Alderete JA, Liu SH, Nasef HS, Law PY, Evans CJ, et al. Oxycodone in the opioid epidemic: High "liking", "wanting", and abuse liability. Cell Mol Neurobiol. 2021;41(5):899–926. doi:10.1007/s10571-020-01013-y

4. Berm EJJ, Risselada AJ, Mulder H, Hak E, Wilffert B. Phenoconversion of cytochrome P450 2D6: The need for identifying the intermediate metabolizer genotype. J Clin Psychiatry. 2013;74(10):1025. doi:10.4088/JCP.13lr08555

5. Preskorn SH, Kane CP, Lobello K, Nichols AI, Fayyad R, Buckley G, et al. Cytochrome P450 2D6 phenoconversion is common in patients being treated for depression: Implications for personalized medicine. J Clin Psychiatry. 2013;74(6):614–21. doi:10.4088/JCP.12m07807

6. Shah RR, Smith RL. Addressing phenoconversion: The Achilles' heel of personalized medicine. Br J Clin Pharmacol. 2015;79(2):222–40. doi:10.1111/bcp.12441

7. Gasche Y, Daali Y, Fathi M, Chiappe A, Cottini S, Dayer P, et al. Codeine intoxication associated with ultrarapid CYP2D6 metabolism. N Engl J Med. 2004;351(27):2827–31. doi:10.1056/NEJMoa041888

8. Kawanishi C, Lundgren S, Agren H, Bertilsson L. Increased incidence of CYP2D6 gene duplication in patients with persistent mood disorders: Ultrarapid metabolism of antidepressants as a cause of nonresponse. A pilot study. Eur J Clin Pharmacol. 2004;59(11):803–7. doi:10.1007/s00228-003-0701-4

9. Rau T, Wohlleben G, Wuttke H, Thuerauf N, Lunkenheimer J, Lanczik M, et al. CYP2D6 genotype: Impact on adverse effects and nonresponse during treatment with antidepressants—a pilot study. Clin Pharmacol Ther. 2004;75(4):386–93. doi:10.1016/j.clpt.2003.12.015

10. Zackrisson AL, Lindblom B, Ahlner J. High frequency of occurrence of CYP2D6 gene duplication/multiduplication indicating ultrarapid metabolism among suicide cases. Clin Pharmacol Ther. 2010;88(3):354–9. doi:10.1038/clpt.2009.216

11. Mahgoub A, Idle JR, Dring LG, Lancaster R, Smith RL. Polymorphic hydroxylation of debrisoquine in man. Lancet. 1977;2(8038):584–6. doi:10.1016/S0140-6736(77)91430-1

12. Eichelbaum M, Spannbrucker N, Steincke B, Dengler HJ. Defective N-oxidation of sparteine in man: A new pharmacogenetic defect. Eur J Clin Pharmacol. 1979;16(3):183–7. doi:10.1007/BF00562059

13. Zanger UM, Raimundo S, Eichelbaum M. Cytochrome P450 2D6: Overview and update on pharmacology, genetics, biochemistry. Naunyn Schmiedebergs Arch Pharmacol. 2004;369(1):23–37. doi:10.1007/s00210-003-0832-2

14. Gaedigk A, Sangkuhl K, Whirl-Carrillo M, Klein T, Leeder JS. Prediction of CYP2D6 phenotype from genotype across world populations. Genet Med. 2017;19(1):69–76. doi:10.1038/gim.2016.80

15. Gaedigk A, Dinh J, Jeong H, Prasad B, Leeder JS. Ten years' experience with the CYP2D6 activity score: A perspective on future investigations to improve clinical predictions for precision therapeutics. J Pers Med. 2018;8(2):15. doi:10.3390/jpm8020015

16. Gaedigk A, Eklund JD, Pearce RE, Leeder JS, Alander SW, Phillips MS, et al. Identification and characterization of CYP2D6*56B, an allele associated with the poor metabolizer phenotype. Clin Pharmacol Ther. 2007;81(6):817–20. doi:10.1038/sj.clpt.6100125

17. Nofziger C, Paulmichl M. Accurately genotyping CYP2D6: Not for the faint of heart. Pharmacogenomics. 2018;19(13):999–1002. doi:10.2217/pgs-2018-0105

18. Gaedigk A, Turner A, Everts RE, Scott SA, Aggarwal P, Broeckel U, et al. Characterization of reference materials for genetic testing of CYP2D6 alleles: A GeT-RM collaborative project. J Mol Diagn. 2019;21(6):1034–52. doi:10.1016/j.jmoldx.2019.06.007

19. Caudle KE, Sangkuhl K, Whirl-Carrillo M, Swen JJ, Haidar CE, Klein TE, et al. Standardizing CYP2D6 genotype to phenotype translation: Consensus recommendations from CPIC and the Dutch Pharmacogenetics Working Group. Clin Transl Sci. 2020;13(1):116–24. doi:10.1111/cts.12692

20. Gaedigk A, Ingelman-Sundberg M, Miller NA, Leeder JS, Whirl-Carrillo M, Klein TE, et al. The Pharmacogene Variation (PharmVar) Consortium: Incorporation of the human cytochrome P450 allele nomenclature database. Clin Pharmacol Ther. 2018;103(3):399–401. doi:10.1002/cpt.910

21. Whirl-Carrillo M, Huddart R, Gong L, Sangkuhl K, Thorn CF, Whaley R, et al. An evidence-based framework for evaluating pharmacogenomics knowledge for personalized medicine. Clin Pharmacol Ther. 2021;110(3):563–72. doi:10.1002/cpt.2350

22. De Kesel PMM, Lambert WE, Stove CP. Alternative sampling strategies for cytochrome P450 phenotyping. Clin Pharmacokinet. 2016;55(2):169–84. doi:10.1007/s40262-015-0306-y

23. Frank D, Jaehde U, Fuhr U. Evaluation of probe drugs and pharmacokinetic metrics for CYP2D6 phenotyping. Eur J Clin Pharmacol. 2007;63(4):321–33. doi:10.1007/s00228-006-0250-8

24. Fuhr U, Jetter A, Kirchheiner J. Appropriate phenotyping procedures for drug metabolizing enzymes and transporters in humans and their simultaneous use in the "cocktail" approach. Clin Pharmacol Ther. 2007;81(2):270–83. doi:10.1038/sj.clpt.6100050

25. Silva AR, Dinis-Oliveira RJ. Pharmacokinetics and pharmacodynamics of dextromethorphan: Clinical and forensic aspects. Drug Metab Rev. 2020;52(2):258–82. doi:10.1080/03602532.2020.1758712

26. Schadel M, Wu D, Otton SV, Kalow W, Sellers EM. Pharmacokinetics of dextromethorphan and metabolites in humans: Influence of the CYP2D6 phenotype and quinidine inhibition. J Clin Psychopharmacol. 1995;15(4):263–9. doi:10.1097/00004714-199508000-00005

27. Capon DA, Bochner F, Kerry N, Mikus G, Danz C, Somogyi AA. The influence of CYP2D6 polymorphism and quinidine on the disposition and antitussive effect of dextromethorphan in humans. Clin Pharmacol Ther. 1996;60(3):295–307. doi:10.1016/S0009-9236(96)90056-9

28. Tennezé L, Verstuyft C, Becquemont L, Poirier JM, Wilkinson GR, Funck-Brentano C. Assessment of CYP2D6 and CYP2C19 activity in vivo in humans: A cocktail study with dextromethorphan and chloroguanide alone and in combination. Clin Pharmacol Ther. 1999;66(6):582–8. doi:10.1053/cp.1999.v66.103401001

29. Strauch K, Lutz U, Bittner N, Lutz WK. Dose–response relationship for the pharmacokinetic interaction of grapefruit juice with dextromethorphan investigated by human urinary metabolite profiles. Food Chem Toxicol. 2009;47(8):1928–35. doi:10.1016/j.fct.2009.05.004

30. Lutz JD, Isoherranen N. Prediction of relative in vivo metabolite exposure from in vitro data using two model drugs: Dextromethorphan and omeprazole. Drug Metab Dispos. 2012;40(1):159–68. doi:10.1124/dmd.111.042200

31. Taylor CP, Traynelis SF, Siffert J, Pope LE, Matsumoto RR. Pharmacology of dextromethorphan: relevance to dextromethorphan/quinidine (Nuedexta®) clinical use. Pharmacol Ther. 2016;164(1):170–82. doi:10.1016/j.pharmthera.2016.04.010

32. von Moltke LL, Greenblatt DJ, Grassi JM, Granda BW, Venkatakrishnan K, Schmider J, et al. Multiple human cytochromes contribute to biotransformation of dextromethorphan in vitro: role of CYP2C9, CYP2C19, CYP2D6, and CYP3A. J Pharm Pharmacol. 1998;50(9):997–1004. doi:10.1111/j.2042-7158.1998.tb06914.x

33. McGinnity DF, Parker AJ, Soars M, Riley RJ. Automated definition of the enzymology of drug oxidation by the major human drug metabolizing cytochrome P450s. Drug Metab Dispos. 2000;28(11):1327–34.

34. Takashima T, Murase S, Iwasaki K, Shimada K. Evaluation of dextromethorphan metabolism using hepatocytes from CYP2D6 poor and extensive metabolizers. Drug Metab Pharmacokinet. 2005;20(3):177–82. doi:10.2133/dmpk.20.177

35. Yu A, Haining RL. Comparative contribution to dextromethorphan metabolism by cytochrome P450 isoforms in vitro: can dextromethorphan be used as a dual probe for both CYP2D6 and CYP3A activities? Drug Metab Dispos. 2001;29(11):1514–20.

36. Pope LE, Khalil MH, Berg JE, Stiles M, Yakatan GJ, Sellers EM. Pharmacokinetics of dextromethorphan after single or multiple dosing in combination with quinidine in extensive and poor metabolizers. J Clin Pharmacol. 2004;44(10):1132–42. doi:10.1177/0091270004269521

37. Grzegorzewski J, Bartsch F, Köller A, König M. Pharmacokinetics of caffeine: a systematic analysis of reported data for application in metabolic phenotyping and liver function testing. Front Pharmacol. 2021;12(1):752826. doi:10.3389/fphar.2021.752826

38. Grzegorzewski J, Brandhorst J, Green K, Eleftheriadou D, Duport Y, Barthorscht F, et al. PK-DB: pharmacokinetics database for individualized and stratified computational modeling. Nucleic Acids Res. 2021;49(D1):D1358–64. doi:10.1093/nar/gkaa990

39. Wyen C, Fuhr U, Frank D, Aarnoutse RE, Klaassen T, Lazar A, et al. Effect of an antiretroviral regimen containing ritonavir-boosted lopinavir on intestinal and hepatic CYP3A, CYP2D6 and P-glycoprotein in HIV-infected patients. Clin Pharmacol Ther. 2008;84(1):75–82. doi:10.1038/sj.clpt.6100452

40. Frank D. Evaluation of pharmacokinetic metrics for phenotyping of the human CYP2D6 enzyme with dextromethorphan [dissertation]. Bonn (Germany): Rheinische Friedrich-Wilhelms-Universität Bonn; 2009.

41. Abdelrahman S, Gotschall R, Kauffman R, Leeder J, Kearns G. Investigation of terbinafine as a CYP2D6 inhibitor in vivo. Clin Pharmacol Ther. 1999;65(5):465–72. doi:10.1016/S0009-9236(99)70065-2

42. Abduljalil K, Frank D, Gaedigk A, Klaassen T, Tomalik-Scharte D, Jetter A, et al. Assessment of activity levels for CYP2D61, CYP2D62, and CYP2D6*41 genes by population pharmacokinetics of dextromethorphan. Clin Pharmacol Ther. 2010;88(5):643–51. doi:10.1038/clpt.2010.137

43. Armani S, Ting L, Sauter N, Darstein C, Tripathi AP, Wang L, et al. Drug interaction potential of osilodrostat (LCI699) based on its effect on the pharmacokinetics of probe drugs of cytochrome P450 enzymes in healthy adults. Clin Drug Investig. 2017;37(5):465–72. doi:10.1007/s40261-017-0497-0

44. Barnhart JW. The urinary excretion of dextromethorphan and three metabolites in dogs and humans. Toxicol Appl Pharmacol. 1980;55(1):43–8. doi:10.1016/0041-008X(80)90218-5

45. Chen R, Zheng X, Hu P. CYP2D6 phenotyping using urine, plasma, and saliva metabolic ratios to assess the impact of CYP2D6*10 on interindividual variation in a Chinese population. Front Pharmacol. 2017;8(1):239. doi:10.3389/fphar.2017.00239

46. Chládek J, Zimová G, Beránek M, Martínková J. In vivo indices of CYP2D6 activity: comparison of dextromethorphan metabolic ratios in 4-h urine and 3-h plasma. Eur J Clin Pharmacol. 2000;56(9–10):651–7. doi:10.1007/s002280000218

47. Demirbas S, Reyderman L, Stavchansky S. Bioavailability of dextromethorphan (as dextrorphan) from sustained-release formulations in the presence of guaifenesin in human volunteers. Biopharm Drug Dispos. 1998;19(8):541–5.

48. Dorado P, González I, Naranjo MEG, de Andrés F, Peñas-Lledó EM, Calzadilla LR, et al. Lessons from Cuba for global precision medicine: CYP2D6 genotype is not a robust predictor of CYP2D6 ultrarapid metabolism. OMICS. 2017;21(1):17–26. doi:10.1089/omi.2016.0166

49. Doroshyenko O, Rokitta D, Zadoyan G, Klement S, Schläfke S, Dienel A, et al. Drug cocktail interaction study on the effect of the orally administered lavender oil preparation Silexan on cytochrome P450 enzymes in healthy volunteers. Drug Metab Dispos. 2013;41(5):987–93. doi:10.1124/dmd.112.050203

50. Duedahl TH, Dirks J, Petersen KB, Romsing J, Larsen NE, Dahl JB. Intravenous dextromethorphan to human volunteers: relationship between pharmacokinetics and anti-hyperalgesic effect. Pain. 2005;113(3):360–8. doi:10.1016/j.pain.2004.11.015

51. Dumond JB, Vourvahis M, Rezk NL, Patterson KB, Tien HC, White N, et al. A phenotype–genotype approach to predicting CYP450 and P-glycoprotein drug interactions with the mixed inhibitor/inducer tipranavir/ritonavir. Clin Pharmacol Ther. 2010;87(6):735–42. doi:10.1038/clpt.2009.253

52. Edwards JE, Eliot L, Parkinson A, Karan S, MacConell L. Assessment of pharmacokinetic interactions between obeticholic acid and caffeine, midazolam, warfarin, dextromethorphan, omeprazole, rosuvastatin, and digoxin in phase 1 studies in healthy subjects. Adv Ther. 2017;34(9):2120–38. doi:10.1007/s12325-017-0601-0

53. Eichhold TH, Greenfield LJ, Hoke SH, Wehmeyer KR. Determination of dextromethorphan and dextrorphan in human plasma by liquid chromatography–tandem mass spectrometry. J Mass Spectrom. 1997;32(11):1205–11.

54. Eichhold TH, McCauley-Myers DL, Khambe DA, Thompson GA, Hoke SH. Simultaneous determination of dextromethorphan, dextrorphan, and guaifenesin in human plasma using semi-automated liquid/liquid extraction and gradient liquid chromatography–tandem mass spectrometry. J Pharm Biomed Anal. 2007;43(2):586–600. doi:10.1016/j.jpba.2006.07.018

55. Gaedigk A. Complexities of CYP2D6 gene analysis and interpretation. Int Rev Psychiatry. 2013;25(5):534–53. doi:10.3109/09540261.2013.825581

56. Hou ZY, Pickle LW, Meyer PS, Woosley RL. Salivary analysis for determination of dextromethorphan metabolic phenotype. Clin Pharmacol Ther. 1991;49(4):410–9. doi:10.1038/clpt.1991.48

57. Hu L, Li L, Yang X, Liu W, Yang J, Jia Y, et al. Floating matrix dosage form for dextromethorphan hydrobromide based on gas-forming technique: in vitro and in vivo evaluation in healthy volunteers. Eur J Pharm Sci. 2011;42(1–2):99–105. doi:10.1016/j.ejps.2010.10.010

58. Jones DR, Gorski JC, Haehner BD, O'Mara EM, Hall SD. Determination of cytochrome P450 3A4/5 activity in vivo with dextromethorphan N-demethylation. Clin Pharmacol Ther. 1996;60(4):374–84.

59. Köhler D, Härtter S, Fuchs K, Sieghart W, Hiemke C. CYP2D6 genotype and phenotyping by determination of dextromethorphan and metabolites in serum of healthy controls and of patients under psychotropic medication. Pharmacogenetics. 1997;7(6):453–61.

60. López M, Guerrero J, Jung-Cook H, Alonso ME. CYP2D6 genotype and phenotype determination in a Mexican Mestizo population. Eur J Clin Pharmacol. 2005;61(10):749–54. doi:10.1007/s00228-005-0038-2

61. Lenuzza N, Duval X, Nicolas G, Thévenot E, Job S, Videau O, et al. Safety and pharmacokinetics of the CIME combination of drugs and their metabolites after a single oral dosing in healthy volunteers. Eur J Drug Metab Pharmacokinet. 2016;41(2):125–38. doi:10.1007/s13318-014-0239-0

62. Montané Jaime LK, Lalla A, Steimer W, Gaedigk A. Characterization of the CYP2D6 gene locus and metabolic activity in Indo- and Afro-Trinidadians: discovery of novel allelic variants. Pharmacogenomics. 2013;14(3):261–76. doi:10.2217/pgs.12.207

63. Myrand S, Sekiguchi K, Man M, Lin X, Tzeng RY, Teng CH, et al. Pharmacokinetics/genotype associations for major cytochrome P450 enzymes in native and first- and third-generation Japanese populations: comparison with Korean, Chinese, and Caucasian populations. Clin Pharmacol Ther. 2008;84(3):347–61. doi:10.1038/sj.clpt.6100482

64. Nagai N, Kawakubo T, Kaneko F, Ishii M, Shinohara R, Saito Y, et al. Pharmacokinetics and polymorphic oxidation of dextromethorphan in a Japanese population. Biopharm Drug Dispos. 1996;17(5):421–33.

65. Nakashima D, Takama H, Ogasawara Y, Kawakami T, Nishitoba T, Hoshi S, et al. Effect of cinacalcet hydrochloride, a new calcimimetic agent, on the pharmacokinetics of dextromethorphan: in vitro and clinical studies. J Clin Pharmacol. 2007;47(10):1311–9. doi:10.1177/0091270007304103

66. Nyunt MM, Becker S, MacFarland RT, Chee P, Scarborough R, Everts S, et al. Pharmacokinetic effect of AMD070, an oral CXCR4 antagonist, on CYP3A4 and CYP2D6 substrates midazolam and dextromethorphan in healthy volunteers. J Acquir Immune Defic Syndr. 2008;47(5):559–65. doi:10.1097/QAI.0b013e3181627566

67. Oh KS, Park SJ, Shinde DD, Shin JG, Kim DH. High-sensitivity liquid chromatography–tandem mass spectrometry for the simultaneous determination of five drugs and their cytochrome P450-specific probe metabolites in human plasma. J Chromatogr B Analyt Technol Biomed Life Sci. 2012;895(1):56–64. doi:10.1016/j.jchromb.2012.03.014

68. Qiu F, Liu S, Miao P, Zeng J, Zhu L, Zhao T, et al. Effects of the Chinese herbal formula Zuojin Pill on the pharmacokinetics of dextromethorphan in healthy Chinese volunteers with CYP2D6*10 genotype. Eur J Clin Pharmacol. 2016;72(6):689–95. doi:10.1007/s00228-016-2048-7

69. Schoedel KA, Pope LE, Sellers EM. Randomized open-label drug–drug interaction trial of dextromethorphan/quinidine and paroxetine in healthy volunteers. Clin Drug Investig. 2012;32(2):157–69. doi:10.2165/11599870-000000000-00000

70. Tamminga W, Wemer J, Oosterhuis B, de Zeeuw R, de Leij L, Jonkman J. The prevalence of CYP2D6 and CYP2C19 genotypes in a population of healthy Dutch volunteers. Eur J Clin Pharmacol. 2001;57(10):717–22. doi:10.1007/s002280100359

71. Yamazaki T, Desai A, Goldwater R, Han D, Howieson C, Akhtar S, et al. Pharmacokinetic effects of isavuconazole coadministration with cytochrome P450 enzyme substrates bupropion, repaglinide, caffeine, dextromethorphan, and methadone in healthy subjects. Clin Pharmacol Drug Dev. 2017;6(1):54–65. doi:10.1002/cpdd.281

72. Zawertailo LA, Tyndale RF, Busto U, Sellers EM. Effect of metabolic blockade on the psychoactive effects of dextromethorphan. Hum Psychopharmacol. 2010;25(1):71–9. doi:10.1002/hup.1086

73. Tricco AC, Lillie E, Zarin W, O'Brien KK, Colquhoun H, Levac D, et al. PRISMA extension for scoping reviews (PRISMA-ScR): checklist and explanation. Ann Intern Med. 2018;169(7):467–73. doi:10.7326/M18-0850

74. Hucka M, Bergmann FT, Chaouiya C, Dräger A, Hoops S, Keating SM, et al. The Systems Biology Markup Language (SBML): language specification for Level 3 Version 2 Core Release 2. J Integr Bioinform. 2019;16(2):0021. doi:10.1515/jib-2019-0021

75. Keating SM, Waltemath D, König M, Zhang F, Dräger A, Chaouiya C, et al. SBML Level 3: an extensible format for the exchange and reuse of biological models. Mol Syst Biol. 2020;16(8):e9110. doi:10.15252/msb.20199110

76. König M. Sbmlutils: Python utilities for SBML [Internet]. Zenodo; 2021. Available from: https://zenodo.org/record/6599299 (accessed 2022 Aug 23).

77. König M, Dräger A, Holzhütter HG. CySBML: a Cytoscape plugin for SBML. Bioinformatics. 2012;28(18):2402–3. doi:10.1093/bioinformatics/bts432

78. König M, Rodriguez N. Matthiaskoenig/cy3sbml: Cy3sbml-v0.3.0 – SBML for Cytoscape [Internet]. Zenodo; 2019. Available from: https://zenodo.org/record/3451319 (accessed 2022 Aug 23).

79. König M. Matthiaskoenig/sbmlsim: SBML simulation made easy (v0.1.14) [Internet]. Zenodo; 2021. Available from: https://zenodo.org/record/5531088 (accessed 2022 Aug 23).

80. Somogyi ET, Bouteiller JM, Glazier JA, König M, Medley JK, Swat MH, et al. libRoadRunner: a high-performance SBML simulation and analysis library. Bioinformatics. 2015;31(20):3315–21. doi:10.1093/bioinformatics/btv363

81. Welsh C, Xu J, Smith L, König M, Choi K, Sauro HM. libRoadRunner 2.0: a high-performance SBML simulation and analysis library. arXiv. 2022; arXiv:2203.01175. doi:10.48550/arXiv.2203.01175

82. Grzegorzewski J, König M. Physiologically based pharmacokinetic (PBPK) model of dextromethorphan [Internet]. Zenodo; 2022. doi:10.5281/zenodo.7025683

83. Smith LP, Hucka M, Hoops S, Finney A, Ginkel M, Myers CJ, et al. SBML Level 3 package: hierarchical model composition, Version 1 Release 3. J Integr Bioinform. 2015;12(3):268. doi:10.2390/biecoll-jib-2015-268

84. Yang J, He MM, Niu W, Wrighton SA, Li L, Liu Y, et al. Metabolic capabilities of cytochrome P450 enzymes in Chinese liver microsomes compared with Caucasian liver microsomes. Br J Clin Pharmacol. 2012;73(2):268–84. doi:10.1111/j.1365-2125.2011.04076.x

85. Storelli F, Desmeules J, Daali Y. Genotype-sensitive reversible and time-dependent CYP2D6 inhibition in human liver microsomes. Basic Clin Pharmacol Toxicol. 2019;124(2):170–80. doi:10.1111/bcpt.13124

86. International Commission on Radiological Protection (ICRP). Basic anatomical and physiological data for use in radiological protection: reference values. ICRP Publication 89. Ann ICRP. 2002;32(3–4):5–265.

87. de Simone G, Devereux RB, Daniels SR, Mureddu G, Roman MJ, Kimball TR, et al. Stroke volume and cardiac output in normotensive children and adults: relations with body size and impact of overweight. Circulation. 1997;95(7):1837–43. doi:10.1161/01.cir.95.7.1837

88. Vander JS. Human physiology: the mechanisms of body function. New York: McGraw-Hill Higher Education; 2001.

89. Herman IP. Physics of the human body. Cham: Springer;2016.

90. Jones H, Rowland-Yeo K. Basic concepts in physiologically based pharmacokinetic modeling in drug discovery and development. CPT Pharmacometrics Syst Pharmacol. 2013;2(8):e63. doi:10.1038/psp.2013.41

91. Registered Nurses' Association of Ontario (RNAO). Nursing best practice guideline: tools for assessing anxiety, depression, and stress (Appendix G) [Internet]. 2022. Available from: https://bpgmobile.rnao.ca (accessed 2022 Aug 23).

92. Kerry N, Somogyi A, Bochner F, Mikus G. The role of CYP2D6 in primary and secondary oxidative metabolism of dextromethorphan: in vitro studies using human liver microsomes. Br J Clin Pharmacol. 1994;38(3):243–8. doi:10.1111/j.1365-2125.1994.tb04348.x

93. Bolger MB, Macwan JS, Sarfraz M, Almukainzi M, Löbenberg R. The irrelevance of in vitro dissolution in setting product specifications for drugs like dextromethorphan subject to lysosomal trapping. J Pharm Sci. 2019;108(1):268–78. doi:10.1016/j.xphs.2018.09.036

94. Moghadamnia AA, Rostami-Hodjegan A, Abdul-Manap R, Wright CE, Morice AH, Tucker GT. Physiologically based modelling of inhibition of metabolism: dextromethorphan vs dextrorphan using quinidine inhibition. Br J Clin Pharmacol. 2003;56(1):57–67. doi:10.1046/j.1365-2125.2003.01853.x

95. Ito T, Kato M, Chiba K, Okazaki O, Sugiyama Y. Estimation of interindividual variability of CYP2D6 activity from urinary metabolic ratios in the literature. Drug Metab Pharmacokinet. 2010;25(3):243–53. doi:10.2133/dmpk.25.243

96. Chiba K, Kato M, Ito T, Suwa T, Sugiyama Y. Inter-individual variability of in vivo CYP2D6 activity in different genotypes. Drug Metab Pharmacokinet. 2012;27(4):405–13. doi:10.2133/dmpk.dmpk-11-rg-078

97. Dickinson GL, Rezaee S, Proctor NJ, Lennard MS, Tucker GT, Rostami-Hodjegan A. Incorporating in vitro metabolism data into clinical trial simulations: dextromethorphan as a model. J Clin Pharmacol. 2007;47(2):175–86. doi:10.1177/0091270006294279

98. Ke AB, Nallani SC, Zhao P, Rostami-Hodjegan A, Isoherranen N, Unadkat JD. PBPK model to predict disposition of CYP2D6 and CYP1A2 substrates in pregnant women. Drug Metab Dispos. 2013;41(4):801–13. doi:10.1124/dmd.112.050161

99. Sager JE, Lutz JD, Foti RS, Davis C, Kunze KL, Isoherranen N. Fluoxetine- and norfluoxetine-mediated complex drug–drug interactions. Clin Pharmacol Ther. 2014;95(6):653–62. doi:10.1038/clpt.2014.50

100. Chen R, Rostami-Hodjegan A, Wang H, Berk D, Shi J, Hu P. PBPK modeling to evaluate single-point plasma phenotyping of CYP2D6. Eur J Pharm Sci. 2016;92(1):131–6. doi:10.1016/j.ejps.2016.07.001

101. Rougée LRA, Mohutsky MA, Bedwell DW, Ruterbories KJ, Hall SD. Impact of hepatocyte-to-plasma pH gradient on prediction of hepatic clearance for CYP2D6 substrates. Drug Metab Dispos. 2016;44(11):1819–27. doi:10.1124/dmd.116.071761

102. Adiwidjaja J, Boddy AV, McLachlan AJ. Refining phenotyping approaches to predict drug clearance: a PBPK simulation study. CPT Pharmacometrics Syst Pharmacol. 2018;7(12):798–808. doi:10.1002/psp4.12355

103. Storelli F, Desmeules J, Daali Y. PBPK modeling for prediction of CYP2D6-mediated gene–drug–drug interactions. CPT Pharmacometrics Syst Pharmacol. 2019;8(8):567–76. doi:10.1002/psp4.12411

104. Machavaram KK, Endo-Tsukude C, Terao K, Gill KL, Hatley OJ, Gardner I, et al. Simulating IL-6 effects on CYP450 substrates in neuromyelitis optica across ethnic populations. AAPS J. 2019;21(3):42. doi:10.1208/s12248-019-0309-y

105. Kim EY, Shin SG, Shin JG. Prediction and visualization of CYP2D6 genotype-based phenotype using clustering algorithms. Transl Clin Pharmacol. 2017;25(3):147–52. doi:10.12793/tcp.2017.25.3.147

106. Rüdesheim S, Selzer D, Fuhr U, Schwab M, Lehr T. PBPK modeling of dextromethorphan to investigate interindividual variability within CYP2D6 activity score groups. CPT Pharmacometrics Syst Pharmacol. 2022;11(4):494–511. doi:10.1002/psp4.12776

107. Steinberg GK, Bell TE, Yenari MA. Dose-escalation safety and tolerance study of dextromethorphan in neurosurgery patients. J Neurosurg. 1996;84(5):860–6. doi:10.3171/jns.1996.84.5.0860

108. Ning M, Duarte JD, Stevison F, Isoherranen N, Rubin LH, Jeong H. Determinants of CYP2D6 mRNA levels in healthy human liver tissue. Clin Transl Sci. 2019;12(4):416–23. doi:10.1111/cts.12632

109. Dalton R, Lee SB, Claw KG, Prasad B, Phillips BR, Shen DD, et al. Interrogation of CYP2D6 structural variant alleles improves genotype–phenotype correlation. Clin Transl Sci. 2020;13(1):147–56. doi:10.1111/cts.12695